Future diversity and lifespan of metazoans under global warming and oxygen depletion

Kunio Kaiho

Department of Earth Science, Graduate School of Science, Tohoku University, Sendai, 980-8578, Japan

Correspondence to: Kunio Kaiho (kunio.kaiho.a6@tohoku.ac.jp)

Abstract. The diversification of metazoans began approximately 700–500 million years ago, evolving from cnidarian-like ancestors into complex groups such as arthropods and vertebrates under dynamic environmental conditions. Throughout Earth's history, abrupt climate fluctuations—driven by large-scale volcanism and meteorite impacts—have repeatedly reshaped global biodiversity. Understanding these historical patterns provides critical insights into the long-term future of life under ongoing and future climate change. Here, I model the future ecosystem diversity of terrestrial metazoans—including insects and tetrapods—and marine metazoans by integrating multiple environmental drivers: solar-luminosity–induced warming, alternating icehouse–greenhouse cycles, progressive declines in atmospheric CO_2 and O_2, abrupt climate fluctuations, and anthropogenic impacts. The results indicate that family-level diversity of terrestrial insects, tetrapods, and marine metazoans—including subterranean and deep-water taxa—will begin to decline approximately 0.5 billion years from now, and ultimately vanish at around 0.9, 0.9, and 1.0 billion years, respectively. These projections hold across models both with and without evolutionary adaptation to extremely low CO_2 and O_2 conditions. The difference in extinction timing between land and ocean reflects lower maximum temperatures in marine environments. The primary driver of gradual biodiversity loss is the long-term reduction of atmospheric CO_2 and O_2 due to the steady increase in solar luminosity. However, extinction is completed by episodic warming events—primarily volcanic in origin—that exceed the thermal tolerance limits of metazoans when superimposed on gradual solar-driven warming. These findings offer a unified quantitative framework for understanding the far-future trajectory and ultimate limits of metazoan biodiversity on Earth.

1 Introduction

Metazoans first appeared and diversified around 700–500 million years ago, evolving from simple cnidarian-like organisms into more complex groups such as arthropods and vertebrates during intervals of rising oxygen and shifts from icehouse to greenhouse climates (Erwin, 2015; Kaiho et al., 2024). After transitioning onto land approximately 400 million years ago, metazoans eventually gave rise to humans (genus *Homo*) roughly 3 million years ago. Despite this long evolutionary history, the future trajectory of metazoan diversity remains poorly understood.

Estimates published after 2010 for the eventual collapse of Earth's biosphere vary widely. Projections based solely on long-term solar-driven warming range from 1.0 to 5.0 Gyr (O'Malley-James et al., 2013; Rushby, 2013; Leconte et al., 2013; Wolf and Toon, 2015). In contrast, CO_2-depletion models predict substantially earlier biosphere loss at 0.84–1.08 Gyr (Rushby, 2015; Ozaki and Reinhard, 2021). Mello and Friaça (2019) argue that thermal limits may delay biosphere collapse to ~1.5 Gyr, whereas atmospheric O_2 is projected to fall to 1% present atmospheric levels (PAL) within 1.08 ± 0.14 Gyr, potentially driving an earlier extinction of metazoans (Ozaki and Reinhard, 2021). Overall, current geosphere–biosphere models suggest a remaining biosphere lifespan of at least ~0.8 Gyr, with ~1.2 Gyr as a plausible median estimate (Jebari and Sandberg, 2022).

A gradual increase in solar luminosity is the primary driver of Earth's far-future climate (Franck et al., 2006; Abe et al., 2011; O'Malley-James et al., 2013; Mello and Friaça, 2019; Ozaki and Reinhard, 2021). Over the next 1.1 Gyr, global mean temperature is projected to rise from 14 °C to ~40 °C (Mello and Friaça, 2019), while atmospheric and oceanic O_2 may decline to ~1% PAL (Ozaki and Reinhard, 2021). By ~1.6 Gyr from now, temperatures may exceed 100 °C, rendering Earth uninhabitable for nearly all forms of life.

This warming accelerates continental weathering, which removes atmospheric CO_2 over timescales of hundreds of thousands of years, triggering cascading biological crises. Declining CO_2 will differentially affect C_3 and C_4 plants because of their distinct photosynthetic pathways: C_4 plants tolerate hotter, drier, low-CO_2 conditions better than C_3 plants. Thus, C_3 plants (including most trees) are expected to decline first, followed by C_4 plants, ultimately leading to collapse of metazoan ecosystems (Reinfelder et al., 2000, 2004; Mello and Friaça, 2019; Ozaki and Reinhard, 2021).

Superimposed on the long-term warming trend are ~0.30–0.35 Gyr cyclic climate rhythms (Scotese et al., 2021; Torsvik et al., 2024; Vérard, 2024), driven primarily by plate-tectonic and mantle processes associated with supercontinent cycles (Heron, 2018). These influence long-term climate through changes in ocean circulation and atmospheric composition and may persist as long as mantle convection and oceans remain active—though future CO_2 depletion may dampen or terminate this cyclicity.

In addition, Earth's climate has repeatedly experienced abrupt perturbations. Large-scale volcanism and asteroid impacts have induced rapid global cooling followed by long-term warming (Kaiho, 2025), triggering mass extinctions throughout the past 500 Myr (Erwin et al., 1987; Sepkoski, 1996; Bambach, 2006; Kaiho, 2022). Because these events unfold over tens to tens of thousands of years—shorter than continental-weathering timescales—they temporarily destabilize climate and can profoundly reshape biodiversity.

Despite their importance, neither cyclic nor abrupt events are incorporated into most long-term future-Earth models, leaving major uncertainties in forecasting Earth's biodiversity trajectory. Here, we integrate both types of events as drivers that impose "step changes" on biodiversity to evaluate how long animal life may persist on Earth.

This study further examines extinction dynamics across superterranean, subterranean, surface-water, and deep-sea habitats. The model combines future projections of temperature, CO_2, and oxygen with established constraints on metazoan thermal and oxygen tolerances and CO_2 effect for plant and climate using six key drivers—anthropogenic crises, long-term warming, cyclic climate rhythms, abrupt events, plant decline, and oxygen depletion—to project the extinction trajectories of insects, terrestrial tetrapods, and marine metazoans over the next 1.5 billion years, informed by their documented diversity patterns throughout the Phanerozoic.

This study further investigates extinction dynamics across superterranean, subterranean, surface-water, and deep-sea habitats. By integrating future projections of temperature, CO_2, and atmospheric oxygen with established physiological limits on metazoan thermal tolerance, oxygen requirements, and CO_2-driven effects on plants and climate, the model employs six major drivers—anthropogenic crises, long-term warming, cyclic climate rhythms, abrupt events, plant decline, and oxygen depletion—to forecast extinction trajectories for insects, terrestrial tetrapods, and marine metazoans over the next 1.5 billion years. These projections are grounded in documented diversity patterns throughout the Phanerozoic.

2 Methods

2.1 Method summary

To project the future lifespan of metazoans on Earth, I developed a multi-step model that integrates relationships derived from past climate behavior and biodiversity dynamics (Fig. 1). A key assumption is that the amplitude of long-term icehouse–greenhouse climate cycles—occurring at ~0.35–0.30 Gyr intervals (Scotese et al., 2021; Torsvik et al., 2024; Vérard, 2024)—will gradually diminish as atmospheric CO_2 declines through enhanced continental weathering; for modeling purposes, these cycles are treated as having 0.30 Gyr intervals. In contrast, major abrupt climatic perturbations capable of triggering mass extinctions are assumed to continue recurring at ~0.094 Gyr intervals, based on the mean recurrence time calculated from age data in Kaiho (2025). Importantly, the specific values chosen for these intervals do not influence the 0.1 Gyr–resolution results presented in the abstract (Fig. 2).

Abrupt events (Equation 9) are treated as independent of long-term climate trends (Equation 10), as their short duration precludes substantial modulation by gradual climate evolution. Combined with physiological constraints on metazoans, these cyclic and abrupt processes are expected to operate similarly in the future. This framework also accounts for the long-term decline in mantle potential temperature (Subsection 2.3), because mantle degassing influences both climatic cyclicity and large-scale extinction events.

A further assumption is that progressive atmospheric CO_2 drawdown—accelerated by intensified continental weathering—will trigger recurrent plant crises, while a concurrent decline in atmospheric oxygen will ultimately lead to the extinction of metazoan life.

The analysis proceeded through the following steps:

A. Baseline reconstruction of historical diversity, climate, and oxygen levels (see Subsection 2.2).

B. Projection of future temperature trends (see Subsection 2.3).

C. Determination of metazoan thermal tolerance limits, where local extinction thresholds are scaled to global mean surface temperature based on latitudinal gradients (see Subsection 2.4).

D. Development of an integrated future-diversity model, combining elements from steps A–C with long-term atmospheric CO_2 and O_2 projections, while accounting for food scarcity effects triggered by the collapse of surface-dwelling metazoans (see Subsection 2.5).

Future changes in metazoan diversity were evaluated under four modeled scenarios:

D1. Conservative Model — assumes no full-scale nuclear conflict and conservative ecological responses without evolutionary adaptation to extreme CO_2 and O_2 deficiency.

D2. New Evolutional Model — incorporates potential evolutionary adaptation to extremely low CO_2 and O_2 levels.

D3. Worst Anthropocene Model — assumes a full-scale nuclear war followed by initial recovery (Kaiho, 2022b, 2023, 2025b).

D4. Continuous Worst Anthropocene Model — includes a full-scale nuclear war and ongoing anthropogenic pressures, resulting in prolonged biodiversity decline.

In addition to the standard simulations, supplementary test cases were conducted in which one causal parameter from steps A–D was held constant at its initial value throughout the entire 1.5 Gyr simulation period under the Conservative Model. These auxiliary simulations are not intended as realistic projections, but rather serve to elucidate the individual contributions of each parameter to the timing of metazoan extinction relative to the baseline models.

All datasets were generated using the equations and baseline data outlined in Subsections 2.2–2.5. All calculations were executed in Microsoft Excel, and the resulting data are presented in the accompanying tables.

2.2 Past diversity, climate, and oxygen baselines

To estimate future metazoan diversity, I compiled past records of global surface temperature and biodiversity. Earth's climate has displayed a recurring 0.35–0.30 Gyr cycle since ~1.0 Gyr ago (Fig. 2), consisting of extended greenhouse phases lasting ~0.2 Gyr followed by shorter ~0.1 Gyr icehouse phases (Scotese et al., 2021; Torsvik et al., 2024; Vérard, 2024). To incorporate this cyclicity, I applied an 8 °C temperature anomaly between icehouse and greenhouse states (Scotese et al., 2021) to the Mello and Friaça model (Fig. 2, Table A1).

I selected the five major mass extinctions, each marked by abrupt environmental disruption and >35% marine genera loss—equivalent to >60% species extinction—based on Bambach (2006) and Kaiho (2022a). Family-level extinction percentages capture severe biodiversity losses across taxa. Marine metazoan family-level extinctions were ~22% (end-

Ordovician), 21% (Late Devonian), 50% (end-Permian), 20% (end-Triassic), and 15% (end-Cretaceous) (Sepkoski, 1982). Terrestrial tetrapod extinctions were 54%, 21%, and 38% at the end-Permian, end-Triassic, and end-Cretaceous, respectively (Table A2; Benton, 2010). Insects experienced 35%, 14%, and 8% extinction across the same events (Table A3; Labandeira and Sepkoski, 1993). Because terrestrial tetrapods and insects originated shortly before the second mass extinction, diversity data are unavailable for the first two events; therefore, average extinction percentages from the five marine and three terrestrial crises were used.

Global temperature anomalies associated with each extinction event follow Kaiho (2022a, 2024, 2025a), based on data from Finnegan et al. (2011), Balter et al. (2008), Huang et al. (2018), Chen et al. (2016), Korte et al. (2009), and Vellekoop et al. (2014) (Table A4). Most of these extinctions were triggered by large-scale volcanism, except the end-Cretaceous event, which was caused by an asteroid impact (Kaiho, 2025a).

Although climate cycles evolve over long timescales, mass extinctions unfold far more abruptly. Both processes contribute to global warming and may therefore shorten the time remaining before the eventual disappearance of metazoans in the distant future.

Projections of future atmospheric O_2 levels and marine and terrestrial biodiversity were guided by patterns observed during the Paleozoic biodiversity maximum. In the early Ediacaran (~0.6 Gyr), atmospheric O_2 was ~0.01 PAL, while marine metazoan diversity was ~0.04 (family level). O_2 increased to ~0.10 PAL (diversity = 0.2) by the late Ediacaran (~0.55 Gyr), to ~0.24 PAL (diversity = 0.4) during the Cambrian Explosion (~0.52 Gyr), and reached ~0.38 PAL (diversity = 1.0) by the end-Ordovician (~0.44 Gyr). Atmospheric O_2 further rose to ~0.86 PAL, with diversity remaining at ~1.0, by the end-Silurian (~0.42 Gyr). Fossil evidence indicates that terrestrial metazoans (insects and tetrapods) first appeared when atmospheric O_2 levels approached ~0.8 PAL (Fig. 3). Although these estimates carry substantial uncertainty, they follow the reconstructions of Krause et al. (2018, 2022), supported by Sperling et al. (2015) (Fig. 2c, Table 1).

The following section uses the positive correlation between atmospheric O_2 and biodiversity to constrain future projections, highlighting that the emergence and diversification of terrestrial metazoans occurred during intervals of elevated oxygen levels.

2.3 Future temperature projections

A coherent framework for projecting future global temperatures is illustrated in Figure 1 (highlighted in pale red, yellow, and green). Surface temperature estimates were generated using long-term warming trends, cyclical climate variations, and abrupt events (Events 1–16, modeled as analogs to the "Big Five" mass extinctions), following Equations 1–7 in this subsection. Mantle temperature is treated as a key control on abrupt events (Equations 4–7). The same pacing of icehouse–greenhouse cycles (~0.3 Gyr intervals) and major abrupt extinction events (~0.094 Gyr intervals) is applied to future climate

projections. The uncertainties associated with these cyclicities provide estimates for the timing of complete metazoan extinction, with error margins of ±0.1 Gyr for climate cycles and ±0.03 Gyr (1σ) for abrupt event timing.

To project future global temperatures, I compiled global mean surface temperature data spanning 2.5 Gyr—including the past 1.0 Gyr and the projected next 1.5 Gyr—and integrated both reconstructed historical variations and future projections (orange curve and red/blue points in Fig. 2). Three major physical drivers were incorporated: long-term solar-driven warming, cyclical climate rhythms, and abrupt climate events.

The Global Average Temperature (GAT) is calculated as:

$$GAT = Ts + \Delta Tc + \Delta Te \quad (1)$$

where Ts is the long-term warming trend mainly driven by increasing solar luminosity; ΔTc is the temperature anomaly associated with climate cycles; and ΔTe is the anomaly associated with abrupt events.

Ts is based on the long-term thermal evolution model of Mello and Friaça (2019), consistent with Franck et al. (2006) and Wolf et al. (2017).

ΔTc is 8 °C maximum gradually decreasing to 0 °C at 1.2 Gyr lasting till >1.5 Gyr during greenhouse periods and 0 °C during icehouse phases. 8 °C is anomaly between icehouse and greenhouse intervals based on Phanerozoic temperature reconstructions by Scotese et al. (2021). The gradual decrease is due to a gradual CO_2 decrease by enhanced continental weathering caused by a gradual solar luminosity increase. Earth's climate history has exhibited a cyclical pattern of 0.35–0.30 Gyr since -1.0 Gyr (Fig. 2). This cycle consists of extended greenhouse phases lasting around 0.2 Gyr, followed by shorter icehouse phases of approximately 0.1 Gyr (Scotese et al., 2021; Torsvik et al., 2024; Vérard, 2024). ΔTc values are adjusted based on the well-known climate model result that a doubling of CO_2 produces a 1.5–4 °C (>66% certainty) and 3 °C (best estimation value) increase in surface temperature (Sherwood et al., 2020; Table A1). Starting from the current global average surface temperature of 14 °C (icehouse state), future temperature variations were projected (Table A1; orange curve in Fig. 2). Because the 0.35–0.30 Gyr climatic periodicity may vary in the future due to mantle cooling and increased solar luminosity, these variations could introduce a maximum uncertainty of 0.1 Gyr in the timing of each metazoan diversity phase. This uncertainty was used to constrain the onset of both the diversity decline and final extinction phases. The 0.1 Gyr discrepancy reflects the relatively short duration of individual icehouse periods. However, this effect is expected to be minor owing to the progressive decline in CO_2 levels and the diminished temperature anomalies during the metazoan crisis interval.

ΔTc is set to a maximum of 8 °C during greenhouse intervals, gradually decreasing to 0 °C by 1.2 Gyr and remaining low thereafter, while icehouse intervals are set to 0 °C. The 8 °C anomaly reflects the icehouse–greenhouse contrast reconstructed for the Phanerozoic (Scotese et al., 2021). The gradual decrease is attributed to decreasing CO_2 caused by enhanced continental weathering under increasing solar luminosity. Earth's past climate exhibits 0.35–0.30 Gyr periodicity

(Fig. 2) composed of ~0.2 Gyr greenhouse and ~0.1 Gyr icehouse intervals (Scotese et al., 2021; Torsvik et al., 2024; Vérard, 2024).

ΔTc values were further refined using the well-established 1.5–4 °C warming expected from CO_2 doubling (Sherwood et al., 2020). Starting from the present 14 °C global temperature, all future variations were projected (Table A1; orange curve in Fig. 2). Although future climatic periodicity may shift due to mantle cooling and increased solar flux, the maximum uncertainty in diversity-phase timing is limited to ~0.1 Gyr, a minor effect because CO_2 decline increasingly suppresses cyclic temperature anomalies.

Temperature anomalies associated with abrupt events were estimated from average values of the five major extinction events, excluding the Permian–Triassic cooling whose magnitude remains uncertain (Kaiho, 2025a). These anomalies decrease through time owing to reduced mantle temperatures and correspondingly reduced CO_2 and SO_2 emissions.

Short-lived (<10 kyr) temperature anomalies substantially affect climate despite their minimal influence on long-term trends. These anomalies are defined as cooling followed by warming (light blue and red points in Fig. 2) based on global SST reconstructions (Kaiho, 2022).

The magnitudes of ΔTe were calculated using experimental data (Kaiho et al., 2022; Kaiho, 2025a) and mantle-dependent emission rates, following:

$$\Delta Te = -8.9 - (-8.9 + 8.9 \times SR) \times 2/3 \quad \text{[cooling cases]} \tag{2}$$

$$\Delta Te = 9.9 \times CR \quad \text{[warming cases]} \tag{3}$$

where −8.9 °C and +9.9 °C are the mean cooling and warming anomalies of past mass extinctions. SR and CR are the relative SO_2 and CO_2 emission rates derived from mantle-temperature–dependent regressions:

$$SR = (0.00108Ts - 0.236)/42.25 \ (r = 0.97) \tag{4}$$

$$CR = \frac{(0.501 \times p)}{0.348},\ p = e^{0.0077Tsill} \ (r = 0.90) \tag{5}$$

The sill temperature after 100 years is calculated by:

$$T_{sill} = (E \times Ti)/(E - Ti \times \ln t_i/t_s) \tag{6}$$

and initial sill (a tabular sheet intrusion from magma) temperature:

$$Ti = Tm \times 1423/1603 \tag{7}$$

Where T_m is mantle temperature, E is activation energy (74 kcal/mol for CO_2 release [Jackson et al., 1995] and 67 kcal/mol for SO_2 [Concer et al., 2017]), t_s and t_i are heating durations, and 1423–1603 K represent typical sill and mantle temperatures. The modern mantle temperature is 1603 K (Mello and Friaça, 2019), and the average initial sill temperature is 1423 K (Aarnes et al., 2010); the 180 K difference reflects typical cooling during sill formation. Equations 4 and 5 represent best-fit curves derived from the heating experiments of Kaiho et al. (2022) and Kaiho (2024). Equations 6 is from the Arrhenius equation on page 174 of IUPAC (1996).

2.4 Metazoan thermal tolerance limits

The upper thermal tolerance limits of terrestrial ectotherms (e.g., amphibians, reptiles, arthropods) range from approximately 45–47 °C in low–mid latitudes (0°–60°) and decline to 35–40 °C in high latitudes (60°–90°) (Sunday et al., 2011; Araújo et al., 2013). Marine ectotherms (e.g., mollusks, fish, crustaceans) exhibit upper limits of 40–45 °C between 35°N and 50°S, decreasing substantially to 10–20 °C toward polar regions (Sunday et al., 2011). Although cold tolerance shows wide variability, upper thermal tolerance tends to be phylogenetically conserved among both ectotherms and endotherms (Araújo et al., 2013).

Across metazoans, temperatures exceeding 45–47 °C on land**,** 40–45 °C in surface oceans, and 42–46 °C across most marine and terrestrial habitats approach the limits at which metabolic processes, protein stability, and membrane integrity begin to fail (Somero, 1995; Pörtner, 2002). These thresholds represent the approximate upper bounds for sustained metazoan survival. In this study, a metazoan species was assumed to go extinct at any latitude if the monthly mean of daily maximum temperatures in the warmest month at its habitat exceeded 46 °C.

Using these physiological limits, extinction threshold temperatures were calculated for four major habitat categories—superterranean (St)**,** subterranean (Ut)**,** surface-water (Sw), and deep-water (Dw) metazoans—across all latitude zones (Fig. 4). These thresholds provide essential constraints for projecting how rising global temperatures will affect the persistence of metazoan life in different ecological environments.

2.4.1 For superterranean (St) metazoans

The extinction thresholds for superterranean (St) metazoans—surface-dwelling terrestrial animals—were estimated using the temperature framework illustrated in Figure 4a. Oceanic climate regions on land were used as reference points because they experience milder and more stable climates than continental interiors. The Global Average surface Temperature at Extinction (GATE) for St metazoans (GATEL; Fig. 1) was determined through the following steps:

1. Upper thermal tolerance definition
   The upper survival limit for St metazoans is set to 46 °C, corresponding to the average Local Daily Maximum Temperature (LDMT) in warm-month oceanic climate zones at 0°, 30°, 60°, and 90° latitude.
2. Use of coastal temperature records
   Coastal climate data were selected because maximum daily temperatures in coastal areas are generally lower than in inland regions, providing a conservative estimate for lethal conditions (dashed oblique lines in Fig. 4).
3. Conversion from LDMT to Local Monthly Maximum Temperature (LMMT)
   A –3 °C correction was applied to convert LDMT to LMMT. This offset reflects the typical difference between monthly mean and daily maximum temperatures during the warmest month, based on observations from coastal

cities including Singapore (~0° N), Shanghai (~30° N), Helsinki (~60° N), and Longyearbyen (~80° N) (Weather Spark).

4. Conversion from LMMT to Local Annual Temperature (LAT)

   LAT was derived by applying a latitudinally dependent correction (ΔLT; Fig. 4). ΔLT values were set to –2 °C, –3.5 °C, –7.5 °C, and –9 °C for ~0°, ~30°, ~60°, and ~80° N, respectively, following temperature differences observed in coastal cities of the eastern Atlantic (Weather Spark).

5. Establishing warm-Earth latitudinal temperature gradients

   The warm-Earth latitudinal gradient of LAT was set to be 20 °C and 14 °C larger than the corresponding sea-surface temperature (SST) gradients of 17 °C and 11 °C from 0° to 90° latitude when GAT is 30 °C and 40 °C, respectively (thin oblique lines in Fig. 4a; Gaskella et al., 2022). These gradients reflect changes in solar incidence associated with Earth's axial tilt.

Common procedure for all metazoan groups

6. Determine GATE from LAT at a representative latitude

   LAT at 37° absolute latitude was used as a proxy for Global Annual Temperature (GAT), because modern GAT (14 °C) closely matches LAT at 37° N in oceanic climate regions (Iwaki and San Francisco; Weather Spark).

7. Calculate extinction thresholds (GATE values)

   GATEL (land), GATES (surface water), GATEU (underground), and GATED (deep water) were derived from LAT at 37°, as shown by open dots in Figure 4.

8. Plot extinction latitudes

   Resulting extinction latitudes (e.g., GATEL30) are illustrated in Figure 2.

The LAT required to induce extinction of St metazoans at each latitude (0°, 30°, 60°, 90°) is calculated using:

$$LAT = 46 - 3 - \Delta LT\ (°C) \quad (8)$$

where ΔLT is the latitude-dependent correction applied when converting LMMT to LAT.

2.4.2 Subterranean (underground) metazoans (Ut)

The extinction thresholds for subterranean metazoans (GATEU) were determined using Figure 4b. Although most modern subterranean organisms inhabit shallow depths (~10 cm), future subterranean metazoans capable of tolerating elevated surface temperatures are expected to retreat to depths of approximately 2.5 m. At this depth, the temperature difference between the Local Monthly Maximum Temperature (LMMT) and the Local Annual Temperature (LAT) is about 2 °C—low enough to allow survival. In contrast, at a depth of 1 m this difference approaches ~8 °C, which is too large for survival (Singh and Sharma, 2017). At depths ≥4 m, soil temperature becomes nearly constant throughout the year. the difference between LDMT and LMMT is less than 1 °C (Singh and Sharma, 2017). In Figure 4b, oblique LAT lines were therefore

plotted 2 °C below the closed 46 °C points, representing lethal thermal limits, for subterranean animals living at a depth of 2.5 m. The warm-Earth latitudinal gradient of LAT was set to be sea-surface temperature (SST) gradients of 11 °C and 5 °C from 0° to 90° latitude when GAT is 40 °C and 50 °C, respectively (thin oblique lines in Fig. 4c; Gaskella et al., 2022).

2.4.3 Surface-water (Sw) metazoans

In the surface ocean, the difference between LDMT and LMMT is less than 1 °C; therefore, the sea-surface LMMT is assumed to equal the LDMT used for land. As a result, extinction thresholds for surface-water metazoans (GATES) are set 3 °C higher than those for terrestrial superterranean metazoans (GATEL), as shown in Figure 4c. The warm-Earth latitudinal gradient of LAT was set to be sea-surface temperature (SST) gradients of 17 °C and 11 °C from 0° to 90° latitude when GAT is 30 °C and 40 °C, respectively (thin oblique lines in Fig. 4c; Gaskella et al., 2022).

2.4.4 Deep-water (Dw) metazoans

Deep-sea temperatures remain highly stable year-round, and therefore Figure 4d does not require multiple oblique LAT lines. Deep-water temperatures were derived from annual surface temperatures at 45° absolute latitudes. The reference extinction threshold is represented by the purple closed circle at 45° latitude (46 °C) in Figure 4d. The resulting deep-water extinction threshold (GATED) corresponds to a global surface temperature of 47 °C, shown by the purple open circle in Figure 4d (Table 5).

2.5 Integrated future diversity model using temperature, oxygen, and CO_2

The future diversity model consists of alternating extinction events and recovery phases (Table 2), which is synthesized from Tables 1 and 4–7. Extinction events include climate-driven crises and food-scarcity events that occur after surface-dwelling metazoans disappear. Each event produces substantial biodiversity loss, whereas recovery phases restore diversity to varying degrees depending on environmental conditions. Before the onset of the C_3 plant crisis, recovery rates are set to 1.0, reflecting complete biodiversity recovery. Once the C_3 plant crisis begins, recovery rates gradually decline as atmospheric CO_2 and O_2 continue to fall, reducing ecosystem resilience and limiting the potential for full recovery.

The calculation procedure is as follows.

First, the modern diversity (number of families) at time 0 for each metazoan group is multiplied by the survival rate for each extinction event (Table 2), yielding the post-event diversity (Event 0 [0E]) (Table A5). Second, this value is multiplied by the corresponding recovery rate to calculate the diversity 0.05 Gyr after the event (0R)—with 0.029 as a special case for Event 0—which is then maintained until immediately before the next event (0A). Third, the value at time 0A is multiplied by

the appropriate recovery rate to obtain the diversity at time 1E. This procedure is applied sequentially for Events 1–16 to project biodiversity from the present to 1.5 Gyr into the future.

Average family-level extinction percentages derived from past mass extinctions were used to project future biodiversity change: 26% for marine metazoans (survival rate 0.74), 37% for terrestrial tetrapods (0.63), and 19% for insects (0.81). When the global average temperature equivalent surface (GATEL) exceeds 37 °C (GATEL30)—the threshold at which low-latitude (0–30°) regions become uninhabitable (Fig. 2)—survival rates are further adjusted using the Extinction Area Rate (EAR [km^2/km^2]) and family-level diversity rate across each latitude (DRL). Major drivers of past mass extinctions include global cooling, global warming, ozone-layer destruction that exposes organisms to harmful short-wavelength UV radiation, ocean acidification, and widespread oceanic anoxia. Under future solar-luminosity-driven warming, prolonged high GAT adds an additional extinction pressure to the baseline values derived from past events (Equation 15). After all surface-dwelling metazoans disappear, diversity is further reduced by applying the Food Scarcity Rate (FS), reflecting the restriction of ecosystems to deep-sea chemosynthetic and subterranean habitats (Equation 9).

Future diversity trajectories are influenced by several interacting processes: the ongoing anthropogenic crisis (Event 0), subsequent abrupt mass-extinction analogs (Events 1–11), the sequential C_3 and C_4 plant crises driven by progressive CO_2 depletion, and the long-term decline in atmospheric oxygen (Fig. 2, Table 2). The C_3 plant crisis is defined at ~0.15 mbar CO_2, and the C_4 plant crisis at ~0.01 mbar CO_2 (Fig. 2). Enhanced continental weathering under warming causes the C_3 plant crisis to begin gradually at 0.4 Gyr and the C_4 crisis at 1.0–1.3 Gyr. These collapses trigger metazoan extinction events of ~40% at 0.9 Gyr and nearly 100% between 0.9 and 1.3 Gyr.

Diversity for each event and recovery interval is calculated as (Table 3):

$$D_{nE} = D_{(n-1)A} \times SRC_n \times FS_n \quad \text{[for events]} \tag{9}$$

$$D_{nR} = D_{(n-1)A} \times RR \quad \text{[for recovery periods]} \tag{10}$$

For Events 1–16, survival-rate components for insects (SRC_I), tetrapods (SRC_T), and marine metazoans (SRC_M) are derived as:

$$SRC_I = 1 - (0.19 + 0.77 \times ERW_{SI} + 0.04 \times ERW_U) \tag{11}$$

$$SRC_T = 1 - (0.37 + 0.6 \times ERW_{ST} + 0.03 \times ERW_U) \tag{12}$$

$$SRC_M = 1 - (0.26 + 0.5 \times ERW_{SM} + 0.24 \times ERWA_D) \tag{13}$$

The survival rate (SR) and recovery rate (RR) represent changes in family-level diversity, calculated relative to modern values of 610 insect families, 315 tetrapod families, and 950 marine metazoan families. SR values for Event 0 are set at 0.95, 0.80, and 0.90, respectively, using extinction data of Kaiho, 2025b and Figure 1 of Kaiho (2022). The constants 0.19, 0.37, and 0.26 represent the average family-level extinction rates during past major mass extinctions. Importantly, mass extinctions are caused not only by global warming but also by reductions in sunlight due to stratospheric aerosols, which induce global cooling, along with decreases in precipitation. Accordingly, the total extinction rate for each metazoan group is

treated as the sum of the past major mass-extinction rate and the additional extinction rate attributable specifically to global warming during future intervals in which excess LDMT conditions exceed 46 °C.

$$ERW = EAR \times DRL \quad (14)$$

DRL is the family-level Diversity Rate transformed from generic diversity across each Latitude band for terrestrial mammals based on 193 × 193 km grid cells (Li et al., 2021) using the method of Kaiho (2022). Calculations of ERW_{ST}, ERW_{SI}, and ERW_{SM} are provided in Table 4.

$ERWA_D$, the extinction rate due to warming and anoxia for marine groups, is defined as:

GAT <36°C (events 1–4, 7): $ERWA_D = 0$

GAT ≥36°C (events 5, 6, 8–11): $ERWA_D = 0.9$ (anoxia-driven)

GAT ≥48°C (events 12–16): $ERWA_D = 1$ (warming-driven) (15)

ERWA is applied only to deep-water metazoans. Relevant temperature thresholds are based on Permian-Triassic deep-ocean extinction conditions.

Food Scarcity Rate (FS) is set as Survival Rate in Table 4 using GAT of GATEL and GATES in Figure 2, because the food resources of subterranean and deep-sea metazoans are largely derived from superterranean and surface-water biota (Tables 2a–2c).

Recovery Rates in Conservative Model (Table 2a; Recovery Rates in New Evolutional Model and Continuous Worst Anthropocene Model are shown in Tables 2b and 2c, respectively):

$$RR_T = RRO \times RRC \times RRW \quad (16)$$

$$RR_M = RRO \times RRC \times RRWA \quad (17)$$

$$RRW_T = SR_S \times 0.95 + SR_U \times 0.05 \quad (18)$$

$$RRWA_M = SR_S \times 0.67 + SR_D \times 0.33 \quad (19)$$

Survival Rates (SR) are obtained from Figure 2 and Table 4.

Oxygen-Based Recovery Rate (RRO)

Terrestrial metazoans:

During the next 0.5 Gyr: RRO = 1.0

During the next 0.5–1.05 Gyr: $RRO = (1.05 - T) \times 1.6$

During the next >1.05 Gyr: RRO = 0.0 (20)

Marine metazoans:

During the next <0.5 Gyr: RRO = 1.0

During the next 0.5–1.0 Gyr: $RRO = 1.4 - T$

During the next 1.0–1.1 Gyr: $RRO = (1.1 - T) \times 4$

During the next >1.1 Gyr: RRO = 0.0 (21)

The thresholds reflect oxygen requirements: >10% PAL for terrestrial animals (Krause et al., 2022) and >1% PAL for marine animals (Sperling et al., 2013; Lyons et al., 2014). Time intervals on RRO are based on average ages shown in Figure 2c (Ozaki and Reinhard, 2021). *T* is the numerical time variable in Gyr.

CO_2-Based Recovery Rate (RRC)

During the next ≤ 0.4 Gyr: RRC = 1.0

During the next 0.4–1.0 Gyr: RRC = 1.4 – *T* [Max], (1.0 – *T*) × 10/6 [Min]

During the next 1.0–1.3 Gyr: RRC = 1.4 – *T* [Max], 0 [Min]

During the next >1.3 Gyr: RRC = 0 (22)

Diversity loss due to CO_2 decline is assumed to proceed linearly from RRC = 1.0 to 0.0 between 0.4 and 1.3 Gyr. All rates are at the family level.

The total extinction rate for each metazoan group is thus modeled as the sum of the past major mass-extinction baseline and the warming-driven extinction that occurs once LDMT exceeds 46 °C.

SRC and FS are applied during extinction events, whereas RR is applied during recovery phases between events. Recovery proceeds until the midpoint between extinction events (typically ~50 Myr). The Past Extinction Rate (PER) reflects abrupt reductions in sunlight caused by stratospheric aerosols, which suppress precipitation in most low-latitude regions and induce global cooling, followed by subsequent warming (Kaiho, 2025).

The Extinction Area Rate (EAR) is determined solely by the 46 °C threshold using Figure 4. When warming-driven extinction occurs within latitude bands of 0–10°, 0–20°, 0–30°, 0–40°, 0–50°, 0–60°, 0–70°, 0–80°, and 0–90°, the EAR values for species are 0.17, 0.34, 0.50, 0.64, 0.76, 0.86, 0.94, 0.98, and 1.00, respectively, assuming equivalent contributions from land and ocean surfaces. EAR for species values are converted to EAR for family values using Figures 1b and 1c of Kaiho (2022). These EAR values are derived from GATEL, GATES, GATEU, and GATED (Section 2.4; Fig. 4; Table 4).

For terrestrial metazoans, the coefficient 0.05 represents the proportion of subterranean families (15 of 315) based on mammalian lineage data (Recknagel and Trontelj, 2021; Benton, 2010), whereas the remaining 0.95 corresponds to surface-dwelling families. For marine metazoans, the coefficient 0.33 reflects the proportion of deep-sea fish families among all marine fish families, based on ~6% of teleost species (the majority of all fish) being restricted to >200 m depth (Miller et al., 2022), scaled using the species–genus–family extinction relationship (Kaiho, 2022). The remaining 0.67 applies to surface-water taxa. The diversities of superterranean and subterranean metazoans change independently due to GAT, whereas the diversities of surface-water and deep-water environments change independently due to both high GAT and low dissolved oxygen, as shown in Equations 11–13 (Fig. 2).

Extinction Area Rate for deep-water metazoans (EAR_D) is influenced by both temperature and dissolved oxygen. High surface temperatures reduce deep-water oxygen concentrations, contributing to deep-sea extinctions during the end-Permian and end-Cenomanian anoxia–euxinia events (e.g., Sun et al., 2012; Kaiho et al., 2013, 2016a). Although deep waters are

cooler, the greatest thermal anomalies occur at the surface, while deep-water temperatures remain relatively stable. Consequently, Equation 15 is used for recovery rate (RR) for marine metazoans because GAT exceed end-Permian highest GAT 36 °C during Events 5, 6, and 8–11.

Although oceanic primary producers are dominated by phytoplankton, both C_3 and C_4 photosynthetic pathways occur in marine environments (Reinfelder et al., 2000, 2004). To approximate the effects of terrestrial plant crises on marine metazoans, equivalent reductions and recovery values are provisionally applied to marine systems, mirroring those used for terrestrial tetrapods under two modeled scenarios.

Complete extinction of metazoans is defined as fewer than 0.4 families on land (30% families / 70% species extinctions) and fewer than 0.2 families in the oceans (18% families / 70% species extinctions), based on Figures 1b and 1c of Kaiho (2022a).

3 Results

3.1 Projected changes in global average surface temperature (GAT)

The temperature modeling methods outlined in Section 2.3 and Equations 1–8 yield the projections shown in Figure 2, indicating a long-term warming trend punctuated by abrupt climate events.

During the Phanerozoic (−0.54 Gyr to present), global average surface temperatures oscillated between ~15°C and 25°C, a range expected to persist until ~0.35 Gyr (Climate Phase A), aside from short-lived perturbations linked to major extinction events. Beyond this interval, temperatures are projected to rise progressively: to 25–30°C by ~0.7 Gyr (Climate Phase B), 30–40°C between ~0.7 and 1.0 Gyr (Climate Phase C), 40–50°C between ~1.0 and 1.3 Gyr (Climate Phase D), and eventually to ~70°C by ~1.5 Gyr (Climate Phase E; orange curve in Fig. 2).

Superimposed on this long-term trend are abrupt climate events associated with large igneous province volcanism and major impact events. Based on recurrence patterns of past events, 16 abrupt events are projected over the next 1.5 Gyr (Section 2.5). These produce short-term deviations from the long-term GAT trajectory, represented by light-blue (cooling) and red (subsequent warming) points in Figure 2. The cooling reflects volcanic SO_2– or impact-injected aerosol forcing, followed by CO_2-driven warming (Kaiho, 2025a; Kaiho and Oshima, 2025).

During future Climate Phase A, abrupt cooling events are expected to reduce global temperatures to ~10–14°C, followed by warming peaks of 30–33°C, occurring four times—mirroring Phanerozoic patterns. Phase B is characterized by minima of 16–18°C and maxima of 33–35°C. Higher temperature envelopes are projected for later phases: 22–26°C and 38–43°C in Phase C, 28–36°C and 45–52°C in Phase D, and 39–55°C and 56–72°C in Phase E (Fig. 2).

Among the modeled abrupt events, Events 2, 5, and 8 produce the fastest warming (<0.1 Myr), corresponding to rapid transitions from icehouse to greenhouse states (Fig. 2). Event 8 reaches temperatures sufficient to eliminate low-latitude

metazoans; Event 9 extends this to low- and mid-latitude taxa; and Event 10 reaches lethal conditions for surface-dwelling metazoans globally (Fig. 2).

3.2 Projected changes in metazoan diversity

Future metazoan diversity changes were estimated using Table 2, as constructed from Tables 1, 4, 5 and A1–A4, which then generate Table A5 and Figure 5. The core calculations follow Equations 9 and 10, with SRC and RR values provided in Tables 2a–2c and 6.

Based on these results, the interval from –1.0 to +1.5 Gyr is divided into five evolutionary phases:

(1) Ancestor Phase (early Climate Phase A, <-0.7 Gyr),

(2) Evolution with mass extinctions (late Phase A and early Phase B, -0.7–0.5 Gyr),

(3) Decline with mass extinctions (late Phases B–C, 0.5–1.0 Gyr), and

(4) Aftermath (Phases D and E, >1.5 Gyr) (Fig. 5).

During Climate Phase A, five future mass extinction events (Events 1–4) are projected, analogous to the past "Big Five" (Events –5 to –1). As in the past Phanerozoic, biodiversity is expected to recover fully after each event. Event 0 (the Anthropogenic Crisis) in the Worst Anthropocene Model reduces surviving families to 580 insects, 221 tetrapods, and 855 marine metazoans, followed by full recovery (Fig. 5; Table A5). In the Continuous Worst Anthropocene Model, these reduced levels persist through all subsequent events, though extinction timing remains unchanged (Fig. 5; Table A5).

During Events 0–4 (0–0.40 Gyr), sharp declines are projected in the Conservative (extinction driven by low oxygen and CO_2) and New Evolutional Models (which assumes higher tolerance for low oxygen and full survival under low CO_2), reducing families from 610 → 494 (insects), 315 → 198 (tetrapods), and 950 → 703 (marine), based on Equations 9–15 (Fig. 5; Table A5). In the Worst Anthropocene Model, Event 0 yields 580, 221, and 855 families. Recovery is complete in all cases except the Continuous Worst Anthropocene Model, where reduced diversity persists (Fig. 5; Table A5).

Large volcanic eruptions or asteroid impacts generate severe cooling followed by abrupt warming, similar to past mass extinctions. Metazoan evolutionary phases correspond to intersections between maximum global temperatures (red dots, Fig. 2) and GAT corresponding to the thermal survival limit of 46°C (Local Daily Maximum Temperature [LDMT]), above which protein denaturation occurs.

From 0.4–0.7 Gyr (Climate Phase B), abrupt warming causes increasingly severe extinctions. Outside these events, diversity declines gradually due to falling O_2 and CO_2 and long-term warming associated with solar luminosity increase. By Period 9R (0.5–0.8 Gyr), insect families fall from 610 → 28, tetrapods from 315 → 14, and marine metazoans from 950 → 87 in the Conservative Model (Fig. 5; Table A5). Diversity falls below half its initial value at 0.65, 0.65, and 0.74 Gyr, respectively (Table 7). The New Evolutional Model yields somewhat higher diversity (Fig. 5).

At Event 10 (~0.9 Gyr; Climate Phase C), global average temperature (GAT) reaches approximately 43°C, reducing insect and tetrapod survival to 3% and 2%, respectively, in the Conservative Model (Table 2), corresponding to the crossing

of the GATEL90 threshold (Fig. 2). All superterranean taxa disappear, while subterranean taxa are able to persist only at high latitudes (60°–90°; Fig. 2). However, even these subterranean survivors—estimated at 0.01 insect families and 0.00 tetrapod families in both the Conservative and Worst Anthropocene Models, and 0.00 insect and 0.00 tetrapod families in the Continuous Worst Anthropocene Model—correspond to zero surviving species (Table A5). Therefore, both superterranean and subterranean lineages go extinct simultaneously at Event 10. The New Evolutional Model yields slightly higher values (0.06 and 0.02 families, respectively), but still results in complete extinction (Table A5).

At Event 10, approximately 0.86 and 0.77 marine metazoan families survive in the Conservative Models and Continuous Worst Anthropocene Model, respectively—translating to only a few species. In contrast, the New Evolutional Model yields 5.5 marine metazoan families (Table A5). At this stage, a few high-latitude surface-water families and a small portion of deep-water families in anoxic conditions remain in the oceans. By Event 11 (~1.0 Gyr), marine families decline to zero in all four models. Therefore, complete marine extinction is projected to occur at ~1.0 Gyr in the Conservative, Worst Anthropocene, and New Evolutional Models, and slightly earlier (~0.9 Gyr) in the Continuous Worst Anthropocene Model.

3.3 Contribution factors

To evaluate the relative influence of global warming, oxygen decline, CO_2 decline, and food scarcity (FS) on the timing of metazoan extinction, I conducted a series of sensitivity experiments in which each factor was removed individually from the Conservative Model.

In the absence of abrupt global warming (i.e., removing the SRC component), the complete extinction of insects, tetrapods, and marine metazoans is delayed by approximately 0.1, 0.1, and 0.05 Gyr, respectively (Table 7; Supplementary Table A6a). When the decline in atmospheric oxygen (RRO) is excluded, the delays are 0.1, 0, and 0 Gyr.

Removing the CO_2 decline (RRC) results in no delay in either of two cases—whether RRC alone is held constant or both RRC and the climatic cycle are held constant (Table 7; Supplementary Table A6b). In this scenario, long-term periodic climate oscillations are assumed to continue unchanged into the future because CO_2 does not decrease (Fig. A1). Similarly, holding the climatic cycle constant alone also produces no delay (Table 7; Supplementary Table A6b). Suppressing gradual warming (RRW = 1) likewise yields delays of 0, 0, and 0 Gyr (Table 7; Supplementary Table A6c). When food scarcity following the extinction of surface metazoans is excluded, the delays are 0.1, 0.1, and 0 Gyr (Table 7; Supplementary Table A6c). Because subterranean and deep-water metazoans inevitably experience food scarcity once surface plants and animals disappear, abrupt global warming and food scarcity function as a combined controlling factor.

Taken together, these experiments show that abrupt global warming is the dominant factor determining the timing of metazoan extinction. In contrast, oxygen decline, CO_2 decline, and gradual warming exert comparatively minor influences, primarily because their effects become substantial only after ~1.0–1.1 Gyr (O_2 decline) and ~1.0–1.3 Gyr (CO_2 decline). Abrupt warming begins to impose strong biological stress earlier—for example, SRC drop to 0.29 and 0.23 for insects and

tetrapods at Event 9 (0.8 Gyr), and to 0.03 and 0.02 at Event 10 (0.9 Gyr) (Table 2). Thus, by ~1.0 Gyr, oxygen and CO_2 levels have not yet become the principal extinction drivers; instead, extreme surface warming—amplified by increased solar luminosity, long-term climate cycles, and large-scale volcanism—emerges as the primary cause of terrestrial metazoan extinction.

The impact of abrupt warming on marine metazoans appears ~0.1 Gyr later than in terrestrial groups. SRC decline to 0.09 at Event 10 (0.9 Gyr) and to 0.08 at Event 11 (1.0 Gyr) (Table 2). This lag occurs because maximum land temperatures (LDMT) exceed mean land temperatures (LMMT) by ~3°C, whereas maximum temperatures in surface waters are nearly identical to LMMT (Figs. 4a, 4c).

The timing of diversity decline to below half of its initial value is delayed by 0.1–0.2 Gyr in simulations without O_2 or CO_2 decline, but not in those without abrupt warming (Table 7). This suggests that while long-term reductions in O_2 and CO_2 gradually suppress metazoan diversity, abrupt warming is the key driver of final extinction. Specifically, abrupt warming events lead to complete metazoan extinction due to sharp declines in SRC.

4 Discussion

4.1 Characteristics of future diversity estimation in this study

A remaining biosphere lifespan of ~1.2 Gyr has been proposed as a plausible median estimate (Jebari and Sandberg, 2022). When only the long-term warming trend driven by gradually increasing solar luminosity is considered (Mello and Friaça, 2019), metazoans go extinct at Event 14 at ~1.3 Gyr for marine taxa and Event 13 at ~1.2 Gyr for terrestrial taxa, based on the intersection of the black dashed line with the upper boundary of GATES90 following the logic in Section 3.2 (Fig. 2). Under the oxygen-depletion scenario of Ozaki and Reinhard (2021), atmospheric O_2 falls below ~0.01 PAL at ~1.1 Gyr—sufficient to induce metazoan extinction. The present study indicates that metazoan demise occurs 0.1 Gyr earlier than estimates based solely on long-term warming and accompanied atmospheric O_2 and CO_2 loss, except for marine metazoans under the New Evolutional Model.

This discrepancy arises because previous models do not incorporate the effects of extreme surface-temperature anomalies linked to mass-extinction–scale events. In contrast, the estimates produced here integrate all major drivers of future temperature variability—long-term warming trends, climatic cyclicity, cooling effects tied to long-term mantle-temperature decline, gradual decreases in O_2 and CO_2, and abrupt catastrophic events—together with group-specific physiology and habitat constraints, providing a more realistic projection of conditions leading to metazoan extinction.

Extinction or survival rates during abrupt events are critical for understanding the fate of particular taxa—including humans—and for determining the final extinction timing of each metazoan group. However, these rates have less influence

on long-term biodiversity trajectories. Instead, recovery rates (RR) under gradual environmental change strongly shape long-term diversity patterns (Equations 9 and 10).

Figure 3 shows a positive relationship between oxygen levels and biodiversity. The emergence of terrestrial metazoans likely required elevated atmospheric oxygen, because survival on land depended on the formation of an ozone layer capable of blocking harmful short-wavelength UV radiation. This dependency provides a possible explanation for why terrestrial insects and tetrapods exhibit lower recovery rates than marine metazoans after ~0.5 Gyr (Fig. 5).

Because comprehensive fossil records for non-insect terrestrial invertebrates are lacking, Figure 5 presents only the diversity trajectories of tetrapods and insects. Nonetheless, most terrestrial invertebrates are expected to follow similar trends, given their comparable upper thermal-tolerance limits. These organisms predominantly occupy surface environments or shallow soil layers, where thermal regimes closely match those experienced by insects and small vertebrates (Somero, 1995; Pörtner, 2002). Therefore, their future biodiversity trajectories are expected to parallel those of terrestrial insects and tetrapods.

Sea-water temperature is uniform at a given location, whereas land temperatures vary depending on sun exposure. Because land temperatures in this study correspond to shaded conditions, the results reflect extinction and survival rates based on the assumption that organisms would die even if they sought refuge in the shade. Thus, the extinction and survival rates presented here are accurate.

4.2 Reliability of future biodiversity projections

Future metazoan diversity is shaped by seven primary forcings:
(1) the long-term increase in solar luminosity,
(2) long-term (0.35–0.30 Gyr) hothouse–icehouse climate cycles,
(3) abrupt climate disruptions linked to major mass-extinction processes,
(4) progressive CO_2 decline,
(5) progressive atmospheric oxygen decline, and
(6) the anthropogenic crisis.
Accordingly, the reliability of future biodiversity projections depends on six key considerations:
(1) whether solar luminosity remains the dominant control on the persistence or extinction of life,
(2) whether long-term hothouse–icehouse cycles continue to operate,
(3) whether abrupt climate perturbations associated with mass-extinction-scale events continue to occur,
(4) whether CO_2 decline induces major plant crises,
(5) whether atmospheric oxygen decline significantly alters metazoan diversity, and

(6) whether life can survive the ongoing anthropogenic crisis, which includes CO_2-driven warming, pollution, deforestation, and the risk of full-scale nuclear conflict.

4.2.1 Solar luminosity increase

The long-term rise in solar luminosity is modeled using a suite of coupled Earth-system components—including mantle convection, quasigrey radiative models, planetary albedo evolution, effective solar flux reconstructions, surface temperature models, atmospheric water-loss processes, continental-weathering feedbacks, and simplified biosphere–climate interactions. These elements, developed by Mello and Friaça (2019) and others, capture essential feedbacks among the atmosphere, hydrosphere, lithosphere, and biosphere, providing a robust basis for projecting future global temperature evolution.

4.2.2 Long-term hothouse–icehouse cycles

Long-term (0.35–0.30 Gyr) climate cycles are reconstructed from sea-surface temperature (SST) estimates based on oxygen-isotope compositions of fossil apatite and calcite, together with evidence of glacial diamictites across multiple paleolatitudes. Over the past ~1 Gyr, three complete long-term cycles have been identified, supporting the assumption that similar cycles will continue (Fig. 5). These cycles were driven primarily by plate-tectonic and mantle processes associated with supercontinent assembly and breakup (Heron, 2018). The expected formation of the next supercontinent, Amasia, around 0.25 Gyr (Yoshida, 2016), aligns with the projected onset of the next major icehouse interval (Fig. 2).

Mantle temperatures are expected to remain sufficiently high to sustain large-scale convection—~1350 °C at present, decreasing to ~1250 °C at 0.7 Gyr and ~1200 °C at 1.0 Gyr (Mello and Friaça, 2019). However, progressive CO_2 depletion due to enhanced continental weathering (driven by rising solar luminosity) will reduce the amplitude of future cycles, diminishing their climatic influence during the intervals when terrestrial and marine metazoan extinctions ultimately occur.

4.2.3 Abrupt climate changes associated with mass extinction events

Abrupt climate changes linked to mass extinction events are inferred from oxygen-isotope records of apatite and calcite associated with the five major mass extinctions. Mantle-temperature projections indicate that plume-related large igneous province volcanism will remain possible, and asteroid impacts are expected to continue occurring at rates inferred from lunar and terrestrial cratering histories (Neukum, 1983; Glikson, 1999; Hartmann et al., 2007; Kaiho and Oshima, 2025). Such high-magnitude, short-duration events will therefore likely persist as sources of abrupt climatic disruption superimposed on long-term warming.

Short-term SO_2, soot, and CO_2 releases exert minimal influence on multimillion-year temperature trends because their climatic impacts typically last <0.1–1.0 Myr. Over geological timescales, natural recovery processes—such as sulfur

deposition and CO_2 drawdown—dampen these perturbations. As a result, long-term warming, cyclical climate fluctuations, and abrupt catastrophic events (as represented in Equation 1) collectively define the global temperature trajectory (Fig. 2).

The upper thermal tolerance limit of metazoans is strongly conserved across lineages owing to protein denaturation at high temperatures (Fig. 4), enabling robust projections of future metazoan decline and extinction.

4.2.4 CO_2 decrease - plant crises

A major C_3 plant crisis is projected to begin around 0.4 Gyr, resulting in widespread loss of trees and associated terrestrial metazoans (Fig. 5; Mello and Friaça, 2019; Ozaki and Reinhard, 2021). This crisis will likely facilitate the expansion of C_4 plants, which use CO_2-concentrating mechanisms and are better adapted to hot, arid, low-CO_2 environments. The resulting ecological shift—from forests to grasslands and eventually to C_4-dominant woody vegetation—will alter recovery rates and contribute to long-term biodiversity decline (RRC in Table 6).

Because both C_3 and C_4 photosynthetic pathways are expected to persist in marine ecosystems (Reinfelder et al., 2000, 2004), the same diversity-recovery rates (RRC) are applied to marine diversity trends, which subsequently exert cascading negative effects on global metazoan biodiversity (Fig. 5).

4.2.5 Progressive oxygen depletion

A long-term decline in atmospheric oxygen will further constrain metazoan metabolism and habitat availability, especially for large or active organisms. This oxygen limitation suppresses biodiversity recovery throughout the 0.5–1.1 Gyr interval (Ozaki and Reinhard, 2021).

4.2.6 Anthropogenic crisis

The Anthropocene crisis may cause a minor mass-extinction peak in the late 21st century (Kaiho, 2022b, 2023). However, metazoans can still survive and recover if CO_2 emissions, pollution, deforestation, and nuclear-war risks are effectively mitigated.

Because the post-Anthropocene trajectory of biodiversity depends heavily on human environmental management, this study models two contrasting conditions:

- full recovery after the anthropogenic crisis (RR = 1.0), and
- no recovery (RR = 0.0), in which biodiversity remains suppressed even though the final extinction timing is unchanged.

4.3 Incomplete recoveries in metazoan diversity

Four major factors are projected to limit the full recovery of metazoan diversity following future mass extinction events occurring after ~0.5 Gyr from now:

1. Anthropogenic Crisis

Human-driven environmental pressures—including CO_2 emissions, pollution, habitat loss, and nuclear conflict risk—are expected to inhibit biodiversity recovery until these impacts subside. Under worst-case scenarios, such as full-scale nuclear war, reduced biodiversity may persist continuously until the final extinction of metazoans.

2. Plant Crisis

The second limiting factor is the long-term decline of terrestrial plants driven by reduced atmospheric CO_2. As CO_2 levels approach the minimum threshold required for photosynthesis, global primary productivity sharply decreases. This reduction in ecosystem energy flow constrains the capacity of both terrestrial and marine systems to sustain diverse metazoan communities, preventing full biodiversity recovery after extinction events.

3. Progressive Oxygen Depletion (0.5–1.1 Gyr)

A gradual decrease in atmospheric oxygen further limits recovery. Lower O_2 concentrations restrict aerobic metabolism and shrink habitable environments, particularly for large or metabolically active organisms. This constraint suppresses metazoan recovery potential throughout the 0.5–1.1 Gyr interval.

4. Rising Global Temperatures During Events 8–10 and Intervening Warm Periods (0.7–0.9 Gyr)

Extreme global temperatures—reaching 44–46 °C during Events 8–10—exceed the upper thermal tolerance of most metazoans. Even during non-event intervals, background temperatures of 36–38 °C (similar to those during the end-Permian extinction) persist, preventing diversification and ecological rebound. These elevated temperatures also promote widespread oceanic anoxia and euxinia, driving deep-sea metazoan extinction.

Together, Factors 2–4 generate sustained declines in metazoan diversity during Events 5–12 (Fig. 5). Factor 1—the anthropogenic crisis—further inhibits recovery for as long as it continues. An interesting implication of this timeline is that the total lifespan of metazoans on Earth is therefore estimated at 1.6–1.7 billion years—approximately 12% of Earth's projected 12-billion-year habitable lifespan. Humanity currently exists near 40% of Earth's metazoan history and about 30% of Earth's terrestrial metazoan history.

4.4 Uncertainties in the timing of final metazoan extinction

Earth's surface temperature is the primary factor controlling the timing of complete metazoan extinction. Consequently, uncertainties in estimating final extinction timing are directly tied to uncertainties in surface temperature. These include components such as the long-term warming trend, long-term climatic cycles (icehouse and greenhouse phases), and abrupt climate shifts.

The uncertainty associated with the long-term warming trend is estimated at −0.1 to +0.2 Gyr, based on Mello and Friaça (2019). Uncertainty from climatic cycles is ±0.1 Gyr; however, this contribution is minor at the point of complete extinction. The timing of abrupt events carries an uncertainty of ±0.03 Gyr (1σ). Additionally, differences in metazoan

responses to declining O_2 and CO_2 levels are reflected in the divergence between survival durations in the Conservative and New Evolutional Models.

Therefore, the total uncertainty in the timing of final metazoan extinction, as governed by Earth's surface temperature, is estimated to range from −0.1 to +0.2 Gyr.

5 Conclusions

Future metazoan diversity will be shaped by the combined impacts of gradual global warming, abrupt climate shifts that trigger major mass extinctions, CO_2-induced plant crises, and progressive atmospheric oxygen depletion. Incorporating these factors, Figure 5 reconstructs metazoan diversity over the past 1 Gyr and projects trends 1.5 Gyr into the future. Despite uncertainties ranging from −0.1 to +0.2 Gyr (Fig. 2 caption), all model scenarios consistently predict a long-term decline in biodiversity beginning around 0.5–0.9 Gyr, ultimately resulting in the extinction of terrestrial metazoans by approximately 0.9 Gyr and marine metazoans by approximately 1.0 Gyr.

A central finding of this study is that abrupt climatic events substantially accelerate the extinction timeline of metazoans. In the absence of such events, the global average surface temperature (GAT) would reach the upper thermal limit for marine metazoans only around ~1.2 Gyr from now, at which point declining atmospheric oxygen and CO_2 would become the dominant extinction drivers. However, when abrupt warming events are included, rapid temperature spikes—superimposed on the long-term reductions in oxygen and CO_2—produce a much earlier and more abrupt collapse of biodiversity. Thus, while slow geochemical feedbacks cause a gradual reduction in metazoan diversity, extreme global warming acts as the primary and immediate trigger of extinction.

For the past 500 million years—and for the next ~400 million years—the Earth system has repeatedly recovered its climate state and biodiversity following abrupt disruptions associated with major mass extinction events. Beyond ~500 million years from now, however, long-term declines in atmospheric oxygen and carbon dioxide will drive a persistent and irreversible reduction in global biodiversity. Although abrupt events do not directly cause this long-term trend, the upper thermal tolerance limit of metazoans will be exceeded for the first time during a future episode of abrupt warming triggered by large-scale volcanic activity.

Such extreme warming events are projected to continue recurring. After roughly 10–11 additional events, the combined effects of solar-luminosity-driven long-term warming and episodic temperature spikes will exceed metazoan thermal limits even at high latitudes, ultimately eliminating all animal life. Subterranean metazoans—which constitute only a small fraction of overall diversity—will disappear simultaneously, while deep-water species will be eliminated by the combined impacts of extreme surface warming and widespread oceanic anoxia.

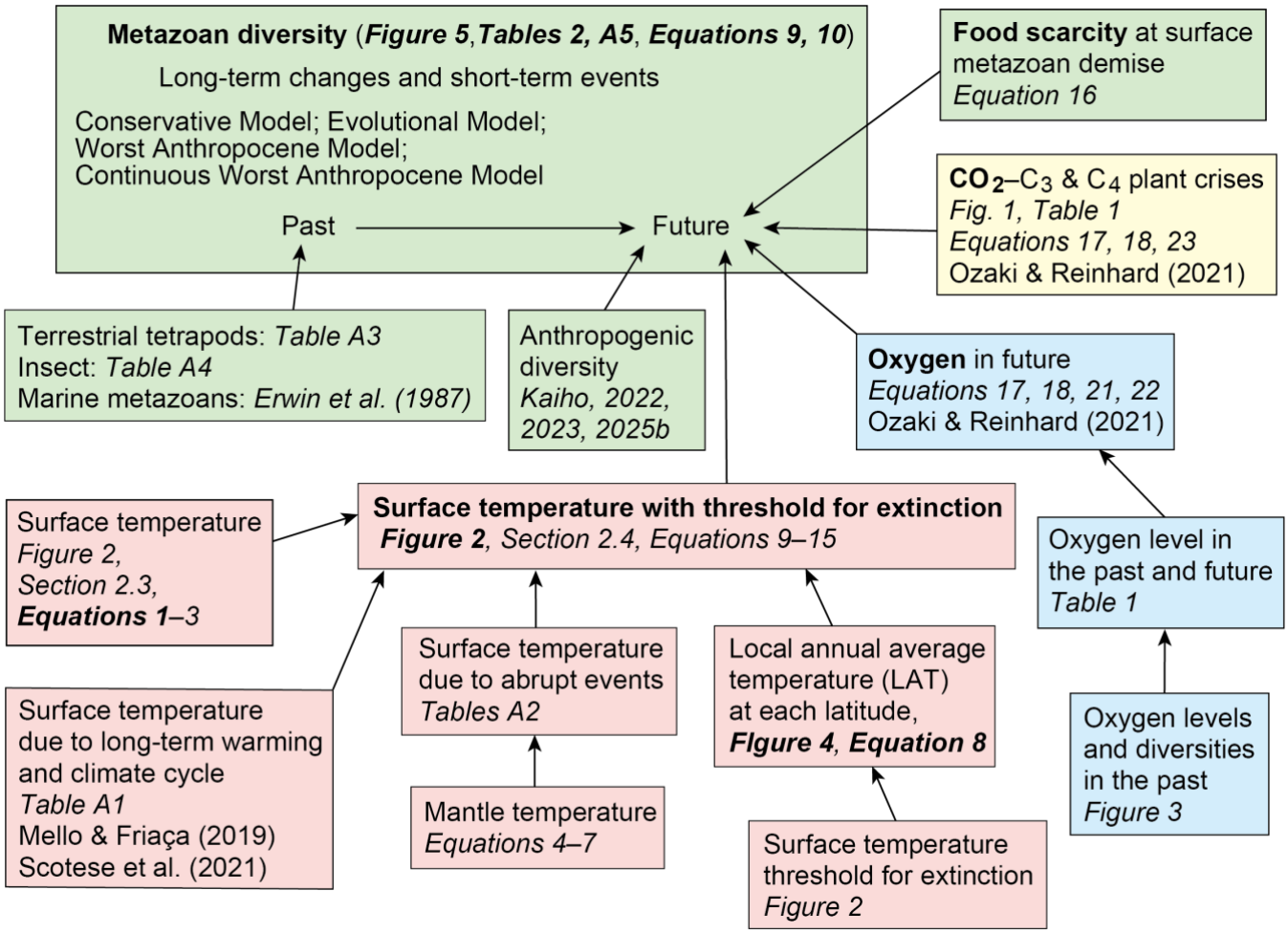

Figure 1. Flowchart illustrating the methodological framework used to estimate past and future metazoan diversity and thereby determine the lifespan of metazoans on Earth. The diagram summarizes the sequential steps leading to the projections shown in Figure 5. Color coding highlights key controlling factors: red indicates temperature, blue represents atmospheric oxygen levels, yellow corresponds to atmospheric CO_2 concentrations, and green denotes metazoan diversity.

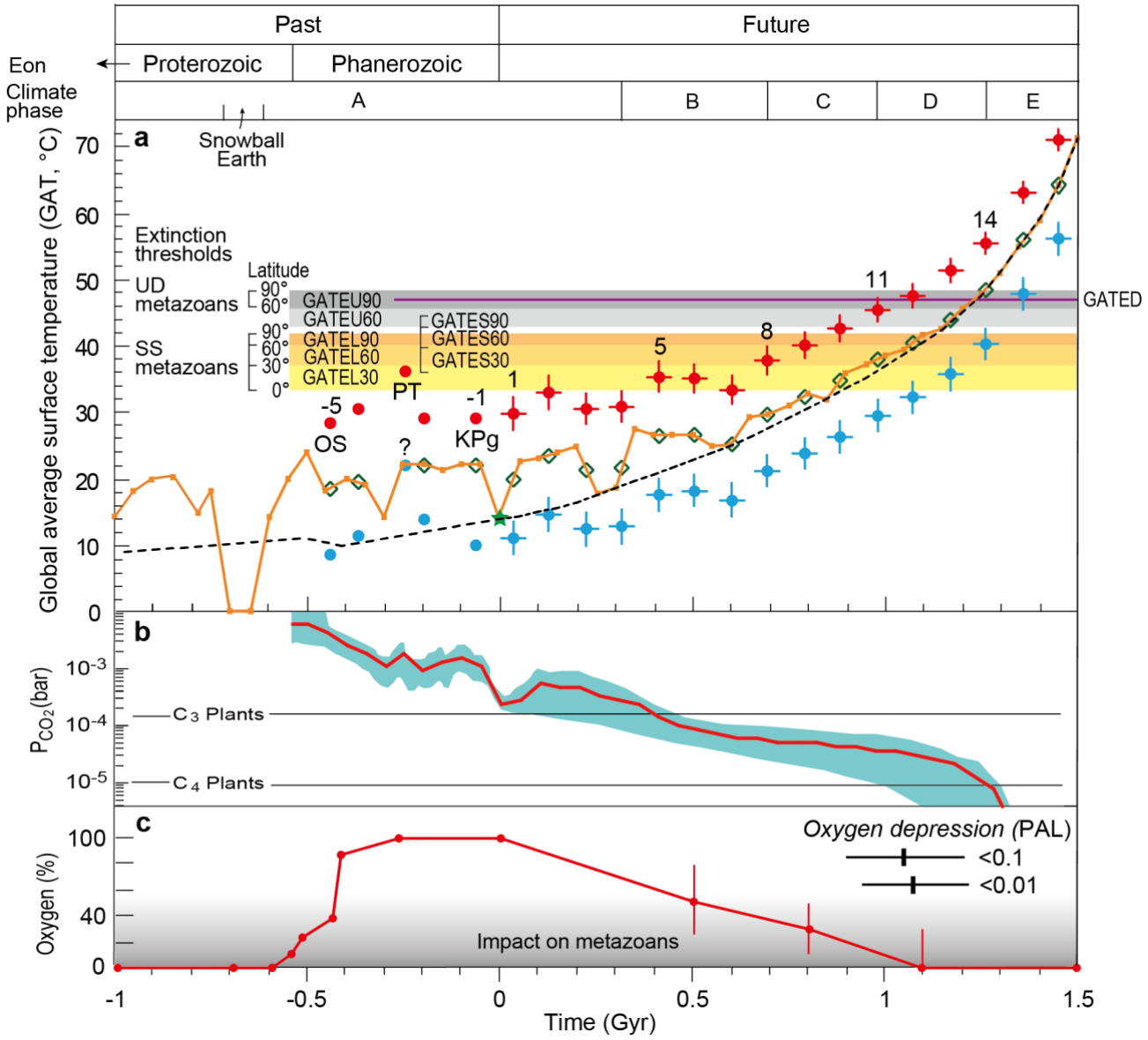

Figure 2. Global average surface temperature and atmospheric CO_2 and oxygen levels over the past and future 2.5 Gyr. Global average surface temperature (a), CO_2 content (b), and atmospheric oxygen levels (c) are shown for the past 1.0 billion years (−1.0 Gyr) and projected for the next 1.5 Gyr (to +1.5 Gyr), together with metazoan extinction thresholds and climate phases. The black dashed line, adapted from Mello and Friaça (2019), represents long-term historical trends (error range: −0.1 to +0.2 Gyr). The orange curve illustrates long-term cyclical icehouse–greenhouse variations (error range: ±0.1 Gyr), based on historical data from Scotese et al. (2021) and estimates for −1.0 to −0.6 Gyr from Vérard (2024) (Table A1). Future projections for both curves begin at the green star marking the modern global average temperature (14 °C). The future portion of the orange curve is calculated from CO_2 content data (b; Table A1).

Light blue and red dots indicate average surface temperatures during major mass extinction events, representing cooling phases (blue) and subsequent warming phases (red) (Kaiho, 2025a; Table A2). Green open diamonds show temperatures immediately preceding each extinction. Vertical error bars denote the standard deviations of temperature anomalies associated with major extinction events (Table A2). The yellow–orange shaded regions (corresponding to open circles in Figure 4) represent upper temperature limits for superterranean and surface-water (SS) metazoan extinction across three latitude bands (0–30°, 30–60°, 60–90°) (GATEL and GATES). Gray shaded regions mark extinction thresholds for subterranean (U) metazoans at 30–60° and 60–90° (GATEU). The extinction threshold for deep-sea (D) metazoans is indicated by the purple horizontal line (GATED; see Fig. 4). "PT" and "KPg" denote the Permian–Triassic and Cretaceous–Paleogene boundary events, while numbers −5, −1, 1, 5, 8, 11, and 14 correspond to event identifiers. Predicted timings of future atmospheric CO_2 and oxygen depletion follow Ozaki and Reinhard (2021). The gray gradient in panel (c) indicates the magnitude of oxygen-related constraints on metazoan diversity (see Equations 21–22 in Section 2.5), with darker shading indicating stronger limitations. PAL refers to Present Atmospheric Level. Past atmospheric oxygen data are from Krause et al. (2018) and Sperling et al. (2015).

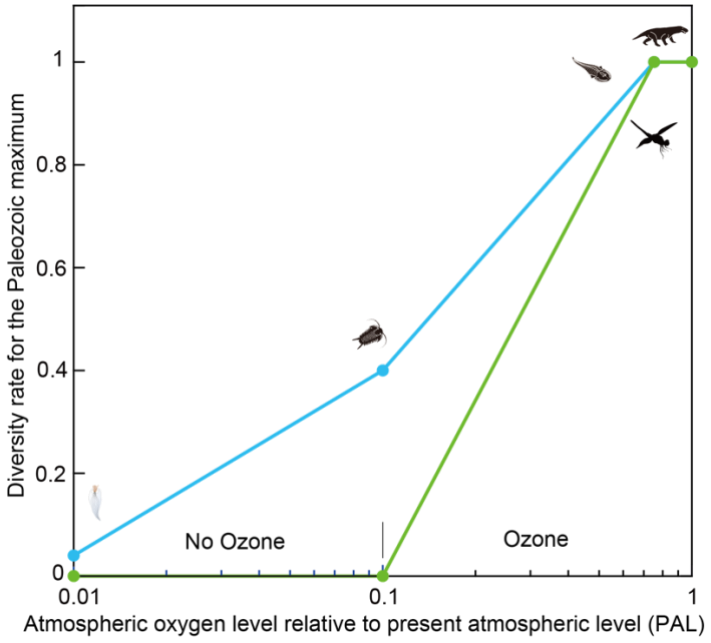

Figure 3. Relationship between atmospheric oxygen levels and past metazoan diversity. This figure illustrates the relationship between atmospheric oxygen concentrations and the diversity of marine metazoans, terrestrial tetrapods, and insects. Blue lines with circular markers show marine metazoan diversity, while pale green lines with square markers represent terrestrial tetrapods and insects. Data span the Neoproterozoic and Paleozoic intervals during which atmospheric oxygen rose substantially. Oxygen level estimates are from Sperling et al. (2015) and Krause et al. (2022), and diversity data derive from Erwin et al. (1987), Labandeira and Sepkoski (1993), Engel and Grimaldi (2004), and Benton (2010). Silhouettes of metazoans depict approximate diversity levels and associated oxygen concentrations.

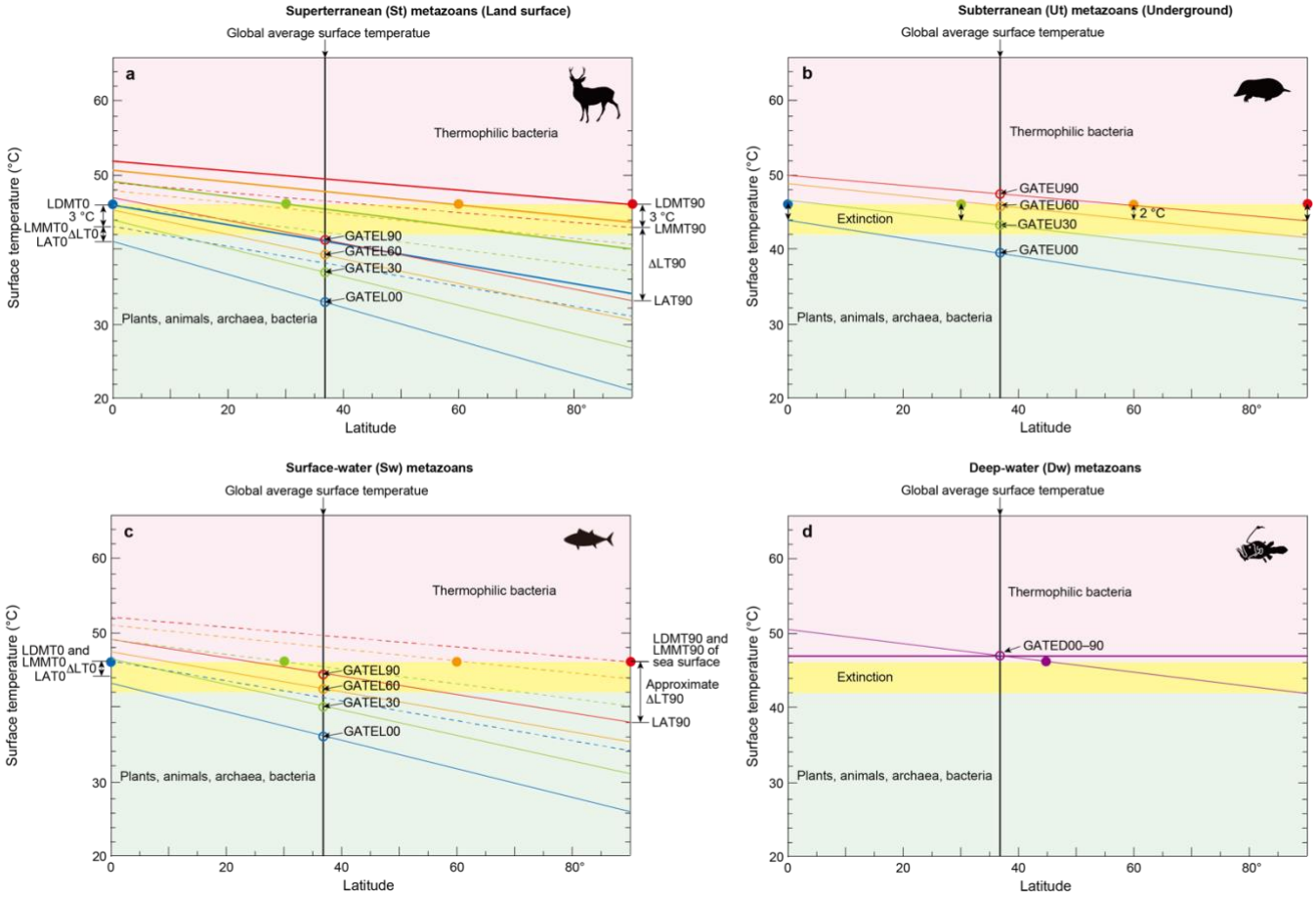

695

Figure 4. Surface temperatures across latitudes corresponding to the extinction thresholds of four metazoan groups.

(a) Global Average surface Temperature (GAT) required for the extinction of superterranean (St; surface-dwelling terrestrial) metazoans (GATEL). Thick oblique lines represent Local Daytime Maximum Temperatures during the warmest month (LDMT). Dashed oblique lines indicate Local Monthly Maximum Temperatures (LMMT), and thin oblique lines indicate Local Average Temperatures (LAT). LT =

700 Local Temperature. Latitudes 0°, 30°, 60°, and 90° are labeled as 00, 30, 60, and 90, respectively. The intersection of the vertical black line at 37° with LAT oblique lines yields the global average surface temperatures GATEL00 to GATEL90. (b) GAT required for the extinction of subterranean (Underground) metazoans (GATEU). (c) GAT required for the extinction of surface-water (Sw) marine metazoans (GATES). (d) GAT required for the extinction of deep-water (Dw) metazoans (GATED). The purple horizontal line represents the upper thermal threshold for deep-water metazoans. Across all panels (a–d), the yellow-shaded region denotes the temperature range

705 capable of causing metazoan extinction, common to both terrestrial and marine groups (Sunday et al., 2011; Araújo et al., 2013). Closed circles mark the maximum extinction temperature (46 °C) at latitudes 0°, 30°, 60°, and 90°. Corresponding open circles, color-matched to the closed markers, indicate the global average temperatures associated with these extinction thresholds. See Methods section 2.4 for details.

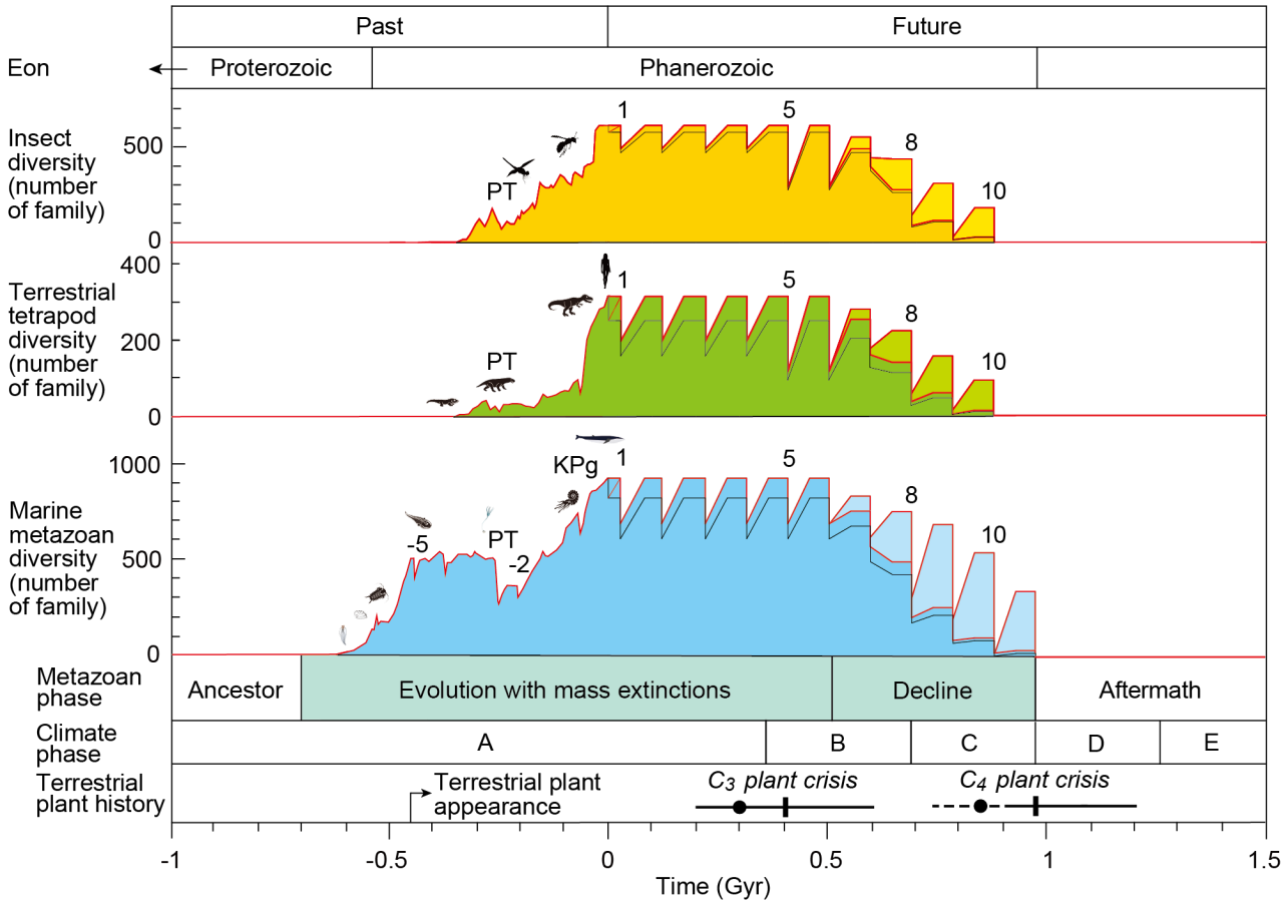

Figure 5. Changes in the diversity of insects, tetrapods, and marine metazoan families based on four environmental–ecological models over the past 1 billion years (Gyr) and projections for the next 1.5 Gyr, alongside metazoan phases, climate phases, and terrestrial plant history. Dark-colored curves show diversity changes under the *Conservative Model*, in which no special evolutionary adaptation occurs in response to future low-oxygen and low-CO_2 conditions (Tables 2a and A5a). Pale-colored curves represent diversity changes under the *New Evolutional Model*, which assumes that metazoans evolve adaptive mechanisms allowing survival under low-oxygen and low-CO_2 conditions in the distant future (Tables 2b and A5b). The negative spikes in the red curves at Event 0 illustrate diversity changes under the *Worst Anthropocene Model*. The black curves represent diversity trajectories under the *Continuous Worst Anthropocene Model*, in which long-term anthropogenic impacts persist through the end of metazoan history (Tables 2c and A5c). Diversity data for geological time are derived from fossil records reported in previous studies (Erwin et al., 1987; Labandeira and Sepkoski, 1993; Engel and Grimaldi, 2004; Benton, 2010; see Tables A2 and A3). Future projections follow survival and recovery rates listed in Table 2. Terrestrial plant crises are modeled using data from Mello and Friaça (2019) (indicated by dots and dashed lines) and Ozaki and Reinhard (2021) (indicated by solid lines). Detailed procedures for future-diversity calculations are provided in the Methods section and illustrated in Figure 1. Abbreviations: PT = Permian–Triassic boundary extinction; KPg = Cretaceous–Paleogene boundary extinction; −5, 1, 5, 8, and 9 = event numbers.

Table 1. Atmospheric oxygen levels and metazoan diversity rates controlled by oxygen from –1 to 1.5 Gyr.

Age	Time (Gyr)	Atmospheric Oxygen level for PAL	Surface-water metazoan diversity rate for Paleozoic maxima	Terrestrial tetrapod diversity rate for Paleozoic maxima
Future	1.5	0.00	0	0
	1.1	0.01	0	0
	0.8	0.30	0.4	0
	0.5	0.50	1	1
Mesozoic	-0.1	1.00	1	1
Paleozoic	-0.27	1.00	1	1
	-0.42	0.86	1	0
	-0.44	0.38	1	0
	-0.52	0.24	0.4	0
Neoproterozoic	-0.55	0.10	0.4	0
	-0.6	0.01	0.04	0
	-0.7	0.01	0	0
	-1	0.01	0	0

Past atmospheric oxygen levels (in PAL) are compiled from Krause et al. (2022) and Sperling et al. (2015), while future oxygen levels are based on projections by Ozaki and Reinhard (2021). Future metazoan diversity rates are estimated from the empirical relationship between atmospheric oxygen levels and metazoan diversity observed in the geological record (Fig. 3). Superterranean metazoan diversity rates in the future are inferred from terrestrial plant diversity trends during the Silurian–Carboniferous interval, reflecting the evolutionary lag between terrestrial plant diversification and the subsequent rise of terrestrial tetrapods (Cascales-Miñana, 2016). PAL = Present Atmospheric Level.

Table 2a. Extinction and recovery model for future projections, showing survival rates at the family level under the Conservative Model.

Event				For Event (short term)				For Recovery (long term), 0.05 Gyr after the event				
Climate phase	Future event	Age (Gyr)	Survival Rate by Climate (SRC)			Food Scarcity Rate (FS)		Recovery Rate (RR)				
								by gradual warming RRW RRWA		by O_2 (RRO)		By CO_2 (RRC) and [NC]
			Insect	Tetrapods	Marine animals	T	M	Terrestrial	M	Terrestrial	M	for All
E	16	1.45	0.00	0.00	0.00	0.01	0.01	0	0	0	0	0
E	15	1.35	0.00	0.00	0.00	0.01	0.01	0	0	0	0	0
E	14	1.26	0.00	0.00	0.00	0.01	0.01	0	0	0	0	0.1
D	13	1.16	0.00	0.00	0.00	0.01	0.01	0.01	0.09	0	0	0.2
D	12	1.07	0.01	0.01	0.00	0.01	0.01	0.17	0.52	0	0	0.3
D	11	0.97	0.02	0.02	0.08	0.01	0.01	0.53	0.70	0.1	0.4	0.4
C	10	0.88	0.03	0.02	0.09	0.01	0.11	0.83	0.70	0.2	0.5	0.5
C	9	0.78	0.29	0.23	0.39	0.33	0.73	1	1	0.4	0.6	0.6
C	8	0.69	0.50	0.39	0.46	0.64	0.87	1	1	0.6	0.7	0.7

B	7	0.60	0.63	0.49	0.74	1	1	1	1	0.7	0.8	0.8
B	6	0.50	0.63	0.49	0.74	0.76	1	1	1	0.9	0.9	0.9
B	5	0.41	0.63	0.49	0.74	0.76	1	1	1	1	1	1
A	4	0.31	0.81	0.63	0.74	1	1	1	1	1	1	1
A	3	0.22	0.81	0.63	0.74	1	1	1	1	1	1	1
A	2	0.12	0.81	0.63	0.74	1	1	1	1	1	1	1
A	1	0.03	0.81	0.63	0.74	1	1	1	1	1	1	1
A	0	0.00	0	0	0	1	1	1	1	1	1	1

Survival rates of 0.63 (terrestrial tetrapods) and 0.81 (insects) are derived from fossil-based estimates in Tables A2 and A3. All other survival rates are obtained from the methodological framework described in Section 2.5. Event 0 represents the Anthropogenic Crisis. Future survival rates for insects are scaled from those of tetrapods using the ratio 0.81/0.63. T: Terrestrial. M: Marine.

Table 2b. Extinction and recovery model for future projections, showing family-level survival rates under the New Evolutional Model.

Event				**For Event (short term)**					**For Recovery (long term), 0.05 Gyr after the event**				
Climate phase	**Future event**	**Age (Gyr)**	**Survival Rate by Climate (SRC)**			**Food Scarcity Rate (FS)**		**Recovery Rate (RR)**					
								by gradual warming RRW RRWA		**by O_2 (RRO)**		**By CO_2 (RRC) and [NC]**
			Insect	**Tetrapods**	**Marine animals**	**T**	**M**	**Terrestrial**	**M**	**Terrestrial**	**M**	**for All**
E	16	1.45	0.00	0.00	0.00	0.01	0.01	0	0	0	0	0
E	15	1.35	0.00	0.00	0.00	0.01	0.01	0	0	0	0	0
E	14	1.26	0.00	0.00	0.00	0.01	0.01	0	0	0	0	1
D	13	1.16	0.00	0.00	0.00	0.01	0.01	0.01	0.09	0	0	1
D	12	1.07	0.00	0.00	0.00	0.01	0.01	0.17	0.52	0	0	1
D	11	0.97	0.01	0.01	0.00	0.01	0.01	0.53	0.70	0.4	0.8	1
C	10	0.88	0.03	0.02	0.09	0.01	0.11	0.83	0.70	0.5	0.8	1
C	9	0.78	0.29	0.23	0.39	0.33	0.73	1	1	0.6	0.8	1
C	8	0.69	0.50	0.39	0.46	0.64	0.87	1	1	0.7	0.9	1
B	7	0.60	0.81	0.63	0.74	1	1	1	1	0.8	0.9	1
B	6	0.50	0.63	0.49	0.74	0.76	1	1	1	0.9	0.9	1
B	5	0.41	0.63	0.49	0.74	0.76	1	1	1	1	1	1
A	4	0.31	0.81	0.63	0.74	1	1	1	1	1	1	1
A	3	0.22	0.81	0.63	0.74	1	1	1	1	1	1	1
A	2	0.12	0.81	0.63	0.74	1	1	1	1	1	1	1
A	1	0.03	0.81	0.63	0.74	1	1	1	1	1	1	1
A	0	0.00	0	0	0	1	1	1	1	1	1	1

This model incorporates adaptive evolution to extremely low atmospheric O_2 and CO_2 levels. Survival rates are derived from Section 2.5 and Table A5. T: Terrestrial. M: Marine.

Table 2c. Extinction and recovery model for future projections, showing family-level survival rates under the Continuous Worst Anthropocene Model, which assumes persistent anthropogenic pressures extending to the end of metazoans.

Event				For Event (short term)					For Recovery (long term), 0.05 Gyr after the event				
Climate phase	Future event	Age (Gyr)	Survival Rate by Climate (SRC)			Food Scarcity Rate (FS)		Recovery Rate (RR)				
								by gradual warming RRW RRWA		by O_2 (RRO)		By CO_2 (RRC) and [NC]
			Insect	Tetrapods	Marine animals	T	M	Terrestrial	M	Terrestrial	M	for All
E	16	1.45	0.00	0.00	0.00	0.01	0.01	0	0	0	0	0
E	15	1.35	0.00	0.00	0.00	0.01	0.01	0	0	0	0	0
E	14	1.26	0.00	0.00	0.00	0.01	0.01	0	0	0	0	0.1
D	13	1.16	0.00	0.00	0.00	0.01	0.01	0.01	0.09	0	0	0.2
D	12	1.07	0.00	0.00	0.00	0.01	0.01	0.17	0.52	0	0	0.3
D	11	0.97	0.01	0.01	0.00	0.01	0.01	0.53	0.70	0.1	0.4	0.4
C	10	0.88	0.03	0.02	0.09	0.01	0.11	0.83	0.70	0.2	0.5	0.5
C	9	0.78	0.29	0.23	0.39	0.33	0.73	1	1	0.4	0.6	0.6
C	8	0.69	0.50	0.39	0.46	0.64	0.87	1	1	0.6	0.7	0.7
B	7	0.60	0.81	0.63	0.74	1	1	1	1	0.7	0.8	0.8
B	6	0.50	0.63	0.49	0.74	0.76	1	1	1	0.9	0.9	0.9
B	5	0.41	0.63	0.49	0.74	0.76	1	1	1	1	1	1
A	4	0.31	0.81	0.63	0.74	1	1	1	1	1	1	1
A	3	0.22	0.81	0.63	0.74	1	1	1	1	1	1	1
A	2	0.12	0.81	0.63	0.74	1	1	1	1	1	1	1
A	1	0.03	0.81	0.63	0.74	1	1	1	1	1	1	1
A	0	0.00	0.95	0.80	0.90	1	1	1	1	1	1	1

Survival rates are sourced from Section 2.5 and Table A5. T: Terrestrial. M: Marine.

745

Table 3. Definitions of abbreviations used in Equations 9–24 (all values represent family-level parameters).

D_{nE}	Diversity at the extinction event n
$D_{(n-1)A}$	Diversity just before event n
D_{nR}	Diversity in recovery at event n
ERW_{ST}	Extinction Rate by short-term Warming for superterranean metazoans
ERW_{SM}	Extinction Rate by short-term Warming for surface-water metazoans
ERW_{U}	Extinction Rate by short-term Warming for subterranean (underground) metazoans
$ERWA_{D}$	Extinction Rate by short-term Warming oceanic Anoxia for deep-water metazoans
SR	Survival Rate
SR_{ST}	Survival Rate of surface terranean metazoans
SR_{SM}	Survival Rate of surface marine metazoans
SR_{U}	Survival Rate of subterranean (underground) metazoans
SR_{D}	Survival Rate of deep-water metazoans
SRC	Survival Rate by Climates
SRC_{T}	Terrestrial SRC
SRC_{M}	Marine SRC
ERW	Extinction Rate by Warming
EAR	Extinction Area Rate in all land and ocean (km^2/km^2)
DRL	Diversity Rate in each Latitude range
FS	Food Scarcity rate
RR	total Recovery Rate
RR_{T}	Terrestrial Recovery Rate
RR_{M}	Marine Recovery Rate
RRO	Recovery Rate under declining atmospheric Oxygen
RRC	Recovery Rate under CO_2 drawdown
RRW	Recovery Rate under long-term Warming conditions
RRW_{T}	RRW for terrestrial metazoans
RRW_{M}	RRW for marine metazoans
RRWA	Recovery Rate under long-term warming and oceanic anoxia
$RRWA_{M}$	RRWA for marine metazoans
$RRWA_{D}$	RRWA for deep-sea metazoans
PER	Past Extinction Rate (section 2.2)
EAR_{S}	Extinction Area Rate for St and Sw metazoans
EAR_{U}	Extinction Area Rate for U metazoans
EAR_{D}	Extinction Area Rate for D metazoans
S	Superterranean and Surface-water metazoans
U	Subterranean (Underground) metazoans
D	Deep-water metazoans

Table 4. Extinction and survival rates at the genus and family levels for each latitudinal range.

a

		Genus level			Family level			
Absolute Latitude	**Area Rate**	**Diversity /area**	**Generic diversity**	**Diversity Rate Mammals**	**Extinction Rate Tetrapods**	**Extinction Rate Marine**	**Survival Rate Tetrapods**	**Survival Rate Marine**
0–90°	1.01	2.19	0.26	1.00	1.00	1.00	0.00	0.00
0–80°	0.99	2.00	0.26	0.99	0.98	0.98	0.02	0.02

0–70°	0.95	1.80	0.25	0.96	0.87	0.91	0.13	0.09
0–60°	0.87	1.59	0.23	0.89	0.67	0.89	0.33	0.11
0–50°	0.77	1.36	0.21	0.80	0.52	0.57	0.48	0.43
0–40°	0.64	1.11	0.18	0.68	0.40	0.39	0.60	0.61
0–30°	0.50	0.86	0.14	0.55	0.36	0.27	0.64	0.73
0–20°	0.34	0.59	0.10	0.38	0.30	0.15	0.70	0.85
0–10°	0.17	0.30	0.05	0.19	0.18	0.12	0.82	0.88

b

Absolute Latitude	Area Rate	Generic diversity /area
80–90°	0.02	0.19
70–80°	0.04	0.20
60–70°	0.08	0.21
50–60°	0.10	0.23
40–50°	0.13	0.24
30–40°	0.14	0.26
20–30°	0.16	0.27
10–20°	0.17	0.29
0–10°	0.17	0.30

The upper portion (table a) shows integrated family-level values derived from genus-level diversity (table b). Genus-level diversity per km² is based on Li et al. (2021), with conversions to family-level diversity following Kaiho (2022), Figure 1.

Table 5. Global Average Temperature for Extinction (GATE) for each habitat type (superterranean, subterranean, surface-water, deep-water) and absolute latitude. Values correspond to thresholds defined from Figure 4 and Section 2.4.

	Temperature (°C)			
Absolute Latitude	Land GATEL	Underground GATEU	Sea surface GATES	Deep water GATED
90°	42	48	44	47
60°	40	46	43	47
30°	37	43	40	47
0°	33	40	36	47

Table 6. Recovery rates for terrestrial and marine metazoans, calculated using Equations 15–22.

Between events	Time (Gyr)	RRO		RRC		RRW_T	RRW_S	RRA_D	RRW_M	Terrestrial	Marine
		Terrestrial	Marine	Terrestrial	Marine	Terrestrial	Surface water	Deep water	Marine	RR_T	RR_M
16–	1.45-1.50	0.00	0.00	0.00	0.00	0.00	0.00	0.00	0.00	0.00	0.00
15–16	1.35–1.45	0.00	0.00	0.00	0.00	0.00	0.00	0.00	0.00	0.00	0.00
14–15	1.26–1.35	0.00	0.00	0.10	0.10	0.00	0.00	0.00	0.00	0.00	0.00
13–14	1.16–1.26	0.00	0.00	0.20	0.20	0.01	0.09	0.10	0.09	0.00	0.00
12–13	1.07–1.16	0.00	0.00	0.30	0.30	0.17	0.73	0.10	0.52	0.00	0.00

11–12	0.97–1.07	0.10	0.40	0.40	0.40	0.53	1.00	0.10	0.70	0.02	0.11
10–11	0.88–0.97	0.20	0.50	0.50	0.50	0.83	1.00	0.10	0.70	0.08	0.18
9–10	0.78–0.88	0.40	0.60	0.60	0.60	1.00	1.00	1.00	1.00	0.24	0.36
8–9	0.69–0.78	0.60	0.70	0.70	0.70	1.00	1.00	1.00	1.00	0.42	0.49
7–8	0.60–0.69	0.70	0.80	0.80	0.80	1.00	1.00	1.00	1.00	0.56	0.64
6–7	0.50–0.60	0.90	0.90	0.90	0.90	1.00	1.00	1.00	1.00	0.81	0.81
5–6	0.41–0.50	1.00	1.00	1.00	1.00	1.00	1.00	1.00	1.00	1.00	1.00
4–5	0.31–0.41	1.00	1.00	1.00	1.00	1.00	1.00	1.00	1.00	1.00	1.00
3–4	0.22–0.31	1.00	1.00	1.00	1.00	1.00	1.00	1.00	1.00	1.00	1.00
2–3	0.12–0.22	1.00	1.00	1.00	1.00	1.00	1.00	1.00	1.00	1.00	1.00
1–2	0.03–0.12	1.00	1.00	1.00	1.00	1.00	1.00	1.00	1.00	1.00	1.00
0–1	0.00–0.03	1.00	1.00	1.00	1.00	1.00	1.00	1.00	1.00	1.00	1.00

Rates incorporate oxygen decline (RRO), CO_2 decline (RRC), and warming/anoxia effects (RRW, RRWA).

Table 7. Estimated ages of complete extinction and 50% diversity loss for insects, tetrapods, and marine metazoans under four primary models and seven hypothetical test scenarios.

Case	Complete extinction age (Gyr)			Half diversity age (Gyr)		
	Insect	Tetrapod	Marine metazoan	Insect	Tetrapod	Marine metazoan
1. Conservative Model	0.88	0.88	0.97	0.65	0.65	0.74
2. No warming event (SRC stable, No FS)	1.02	1.02	1.12	0.65	0.65	0.74
3. No O_2 decrease (RRO stable)	0.97	0.88	0.97	0.84	0.84	0.84
4. No CO_2 decrease (RRC stable only)	0.88	0.88	0.97	0.74	0.74	0.84
5. No CO_2 decrease (RRC stable, No decrease climatic cycle)	0.88	0.88	0.97	0.74	0.74	0.84
6. No CO_2 decrease (No decrease climatic cycle only)	0.88	0.88	0.97	0.74	0.74	0.84
7. No gradual warming (RRW stable)	0.88	0.88	0.97	0.65	0.65	0.74
8. No food scarcity (No FS only)	0.97	0.97	0.97	0.65	0.65	0.74
9. Worst Anthropocene Model	0.88	0.88	0.97	0.65	0.65	0.74
10. Continuous Worst Anthropocene Model	0.88	0.88	0.97	0.65	0.65	*0.65*
11. New Evolutional Model	0.88	0.88	0.97	0.74	0.84	0.93

Underlined values indicate delays relative to the Conservative Model, while italicized values indicate earlier occurrences. Cases 2–10 are modified versions of the Conservative Model, among which Cases 2–8 represent hypothetical test scenarios that are not considered realistic.

Acknowledgments

I thank anonymous referees for their valuable comments.

Authorship contributions

Kunio Kaiho: Conceptualization, Formal analysis, Investigation, Methodology, Writing – original draft, Writing – review and editing.

Competing interest declaration

The author declares no competing interests.

Supplementary material

Supplementary material related to this article can be found on-line at https://doi .org/----

Data availability statement

Data is provided within the manuscript or supplementary information files.

References

Aarnes, I, Svensen, H., Connolly, J. A. D., and Podladchikov, Y. Y.: How contact metamorphism can trigger global climate changes: Modeling gas generation around igneous sills in sedimentary basins, Geochim. Cosmochim. Acta, 74, 7179–7195, doi:10.1016/j.gca.2010.09.011, 2010.

Abe, Y., Abe-Ouch, A., Sleep, N. H., and Zahnle, K. J.: Habitable zone limits for dry planets, Astrobiol., 11, 443–460, 2011.

Alexander J. K., Mills, B. J. W., Merdith, A. S., Lenton, T. M., Poulton, S. W. Extreme variability in atmospheric oxygen levels in the late Precambrian. Sci. Adv. 8, eabm8191, DOI: 10.1126/sciadv.abm8191 (2022)

Araújo, M. B., Ferri-Yáñez, F., Bozinovic, F., Marquet, P. A., Valladares, F., Chown, S. L.**:** Heat freezes niche evolution, Ecol. Lett., 16, 1206–1219, doi:10.1089/ast.2010.0545, 2013.

Balter, V., Renaud, S., Girard, C., and Joachimski, M. M.: Record of climate-driven morphological changes in 376 Ma Devonian fossils, Geology, 36, 907–910, doi:10.1130/G24989A.1, 2008.

Bambach, R. K.: Phanerozoic biodiversity mass extinctions, Ann. Rev. Ear. Planet. Sci., 34, 127–155, https://doi.org/10.1146/annurev.earth.33.092203.122654, 2006.

Benton, M. J.: The origins of modern biodiversity on land, Phil. Trans. R. Soc. B 365, 3667–3679, doi:10.1098/rstb.2010.0269, 2010.

Cascales-Miñana, B.: Apparent changes in the Ordovician–Mississippian plant diversity, Rev. Palaeobotany Palynol. 227, 19–27, doi:10.1016/j.revpalbo.2015.10.005, 2016.

Chen, J., Shen, S., Li, X., Xu, Y., Joachimski, M. M., Bowring, S. A., Erwin, D. H., Yuan, D., Chen, B., Zhang, H., Wang, Y., Cao, C., Zheng, Q., and Mu, L.: High-resolution SIMS oxygen isotope analysis on conodont apatite from South

China and implications for the end-Permian mass extinction, Palaeogeogr. Palaeoclimatol. Palaeoecol., 448, 26–38, doi:10.1016/j.palaeo.2015.11.025, 2016.

Concer, P. H., de Oliveira, C. M., Montedo, O. R. K., Angioletto, E., Peterson, M., Fiori, M. A., Moreira, R. de F. P. M.: Kinetics of the oxidation reactions and decomposition of pyrite, Ceramica 63, 39-43, 2017.

Engel, M. S. and Grimaldi D. A.: New light shed on the oldest insect, Nature 427, 627-630, doi:10.1038/nature02291, 2004.

Erwin, D. H.: Early metazoan life: divergence, environment and ecology, Phil. Trans. R. Soc., B 370, 20150036, doi:10.1098/rstb.2015.0036, 2015.

Erwin, D. H., Valentine, J. W., and Sepkoski, Jr.: A comparative study of diversification events: the early Paleozoic versus the Mesozoic, Evolution, 41, 1177–1186, 1987.

Finnegan, S. Bergmann, K., Eiler, J. M., Jones, D. S., Fike, D. A., Eisenman, I., Hughes, N. C., Tripati, A. K., and Fischer, W. W.: The magnitude and duration of Late Ordovician–Early Silurian glaciation. Science, 331, 903–906, doi: 10.1126/science.1200803, 2011.

Franck, S., Bounama, C. and von Bloh, W.: Causes and timing of future biosphere extinctions, Biogeosci., 3, 85–92, doi: 10.5194/bg-3-85-2006, 2006.

Gaskella, D. F., Huber, M., O'Brien, C. L., Inglis, G. N., Acostae, R. P., Poulsene, C. J., and Hull, P. M.: The latitudinal temperature gradient and its climate dependence as inferred from foraminiferal δ18 O over the past 95 million years, Proc. Natl. Acad. Sci. U.S.A., 119, e2111332119, https://doi.org/10.1073/pnas.2111332119, 2022.

Glikson, A. Y.: Oceanic mega-impacts and crustal evolution, Geology, 27, 387–390. doi: 10.1130/0091-7613(1999)027<0387:OMIACE>2.3.CO;2, 1999.

Hartmann, W. K., Quantin, C., Mangold, N. Possible long-term decline in impact rates: 2. Lunar impact-melt data regarding impact history, Icarus 186, 11–23, doi:10.1016/j.icarus.2006.09.009, 2007.

Heron, P. J.: Mantle plumes and mantle dynamics in the Wilson cycle, Geol. Soc. Lond. Spec. Publ., 470, 87–103, doi: 10.1144/SP470-2018-97, 2018.

Huang, C., Joachimski, M. M., and Gong, Y.: Did climate changes trigger the late Devonian Kellwasser Crisis? Evidence from a high-resolution conodont $\delta^{18}O_{PO4}$ record from South China, Earth Planet. Sci. Lett., 495, 174–184, doi:10.1016/j.epsl.2018.05.016, 2018.

IUPAC: A glossary of terms used in chemical kinetics, including reaction dynamics. Pure and Applied Chemistry, 68, 149–192, 1996.

Jackson, K. J., Burnham, A. K., Braun, R. L., and Knauss, K. G. Temperature and pressure dependence of n-hexadecane cracking, *Org. Geochem.*, 23, 941–953, doi: 10.1016/0146-6380(95)00068-2, 1995.

Jebari, K. and Sandberg, A.: Ecocentrism and Biosphere Life Extension, Science and Engineering Ethics, 28, 46, doi:10.1007/s11948-022-00404-2, 2022.

Kaiho, K.: Relationship between extinction magnitude and climate change during major marine and terrestrial animal crises, Biogeosci., 19, 3369–3380, doi:10.5194/bg-2022-29, 2022a.

Kaiho, K.: Extinction magnitude of animals in the near future, Sci. Rep., 12, 19593, doi: 10.1038/s41598-022-23369-5, 2022b.

Kaiho, K.: An animal crisis caused by pollution, deforestation, and warming in the late 21st century and exacerbation by nuclear war, Heliyon, 9, e15221, doi:10.1016/j.heliyon.2023.e15221, 2023.

Kaiho, K.: Role of volcanism and impact heating in mass extinction climate shifts, Sci. Rep., 14, 9946, doi:10.1038/s41598-024-60467-y, 2024.

Kaiho, K.: Mechanisms of global climate change during the five major mass extinctions. Sci. Rep. 15, 16498, doi: 10.1038/s41598-025-01203-y, 2025a.

Kaiho, K.: Integrating climate biodiversity and food security risks from soot injection scenarios. SSRN: http://ssrn.com/abstract=5418361, 2025b.

Kaiho, K., Katabuchi, M., Oba, M., and Lamolda, M.: Repeated anoxia-extinction episodes progressing from slope to shelf during the latest Cenomanian, Gondwana Res., 25, 1357–1368, doi:10.1016/j.gr.2012.12.008, 2013.

Kaiho, K. and Oshima, N.: The significance of impact-induced hydrocarbon soot aerosols in global climate change and extinctions, Palaeogeogr. Palaeoclimatol. Palaeoecol. doi: 10.1016/j.palaeo.2025.113237, 678, 113237, 2025.

Kaiho, K., Saito, R., Oba, M., Ito, K., Miyaji, T., Biswas, R., Tian, L., Sano, H., Shi, Z., Takahashi, S., Tong, J., Liang, L., Oba, M., Nara, F. W., Tsuchiya, N., and Chen, Z.-Q.: Effects of soil erosion and anoxic–euxinic ocean in the Permian–Triassic marine crisis, Heliyon, 2, e00137, doi:10.1016/j.heliyon.2016e00137, 2016a.

Kaiho, K., Tanaka, D., Richoz, S., Jones, D. S., Saito, R., and Kameyama, D.: Volcanic temperature changes modulated volatile release and climate fluctuations at the end-Triassic mass extinction, Earth Planet. Sci. Lett., 579, 117364, doi:10.1016/j.epsl.2021.117364, 2022.

Kaiho, K. and Oshima, N. The significance of impact-induced hydrocarbon soot aerosols in global climate change and extinctions. Palaeogeogr. Palaeoclimatol. Palaeoecol. 113237, 2025.

Kaiho, K., Oshima, N., Adachi, K., Adachi, Y., Mizukami, T., Fujibayashi, M., and Saito, R.: Global climate change driven by soot at the K–Pg boundary as the cause of the mass extinction, Sci. Rep., 6, 28427, doi :10.1038/s41598-017-14199-x, 2016b.

Kaiho, K., Shizuya, A., Kikuchi, M., Komiya, T., Chen, Z-Q., Tong, J., Tian, L., Gorjan, P., Takahashi, S., Baud, A., Grasby, S.E., Saito, R., and Saltzman, M.R.: Oxygen increase and the pacing of early animal evolution, Glob. Planet. Chang., 233, 104364, doi: 10.1016/j.gloplacha.2024.104364, 2024.

Korte, C., Hesselbo, S. P., Jenkyns, H. C., Rockaby, R. E., and Spoetl, C.: Palaeoenvironmental significance of carbon- and oxygen-isotope stratigraphy of marine Triassic–Jurassic boundary sections in SW Britain, J. Geol. Soc., London, 166, 431–445, doi:10.1144/0016-76492007-177, 2009.

Krause, A. J., Mills, B. J. W., Merdith, A. S., Lenton, T. M., and Poulton S. W.: Extreme variability in atmospheric oxygen levels in the late Precambrian, Sci. Adv. 8, eabm8191, doi: 10.1126/sciadv.abm8191, 2022.

Krause, A. J., Mills, B. J. W., Zhang, S., Planavsky, N. J., Lenton, T. M., and Poulton S. W.: Stepwise oxygenation of the Paleozoic atmosphere, Nat. Commun., 9, 4081, doi:10.1038/s41467-018-06383-y, 2018.

Leconte, J., Forget, F., Charnay, B., Wordsworth, R., and Pottier, A.: Increased insolation threshold for runaway greenhouse processes on Earth-like planets. Nature 504, 268–271, 2013.

Li, Y., Wang, S., Cheng, C., Zhang, J., Wang, S., Hou, X., Liu, X., Yang, X., and Li, X.: Latitudinal gradients in genetic diversity and natural selection at a highly adaptive gene in €b0terrestrial mammals, Ecography 44, 206-218, doi: 10.1111/ecog.05082, 2021.

Lyons, T. W., Reinhard, C. T. & Planavsky, N. J. The rise of oxygen in Earth's early ocean and atmosphere. Nature 506, 307–315 (2014).

Mello F. S. and Friaça A. C. S.: The end of life on Earth is not the end of the world: converging to an estimate of life span of the biosphere? Internat. J. Astrobiol., 19, 25–42, doi:10.1017/S1473550419000120, 2019.

Miller, E. C., Martinez, C. M., Friedman, S T., Wainwright, P. C., Price, S. A., and Tornabene, L.: Alternating regimes of shallow and deep-sea diversification explain a species-richness paradox in marine fishes, Proc. Natl. Acad. Sci. U.S.A., 119, e213544119, doi:10.1073/pnas.2123544119, 2022.

Neukum, G.: Meteoritenbombardement und Datierung planetarer Oberflaechen. Habilitation Dissertation, Ludwig-Maximilians-University, Munich, p. 186, 1983.

O'Malley-James, J. T., Greaves, J. S., Raven, J. A., and Cockell, C. S.: Swansong biospheres: refuges for life and novel microbial biospheres on terrestrial planets near the end of their habitable lifetimes, Int. J. Astrobiol., 12, 99–112, doi:10.48550/arXiv.1210.5721, 2013.

Ozaki, K. and Reinhard, C. T.: The future lifespan of Earth's oxygenated atmosphere, Nat. Geosci., 14, 138–142, doi: 10.1038/s41561-021-00693-5, 2021.

Pörtner, H. O.: Climate variations and the physiological basis of temperature-dependent biogeography: systemic to molecular hierarchy of thermal tolerance in animals, Comparative Biochem. Physiol. Part A: Molecul. Integrative Physiol., 132, 739–761, doi:10.1016/S1095-6433(02)00045-4, 2002.

Rushby, A. J., Claire, M. W., Osborn, H., and Watson A. J. Habitable zone lifetimes of exoplanets around main sequence stars. Astrobiology, 13, 833–849, 2013.

Rushby, A. J.: Modelling biogeochemical controls on planetary habitability. PhD Thesis, University of East Anglia, 2015.

Recknagel, H. and Trontelj, P.: From cave dragons to genomics: advancements in the study of subterranean tetrapods, BioScience, 72, 254–266, doi:10.1093/biosci/biab117, 2021.

Reinfelder, J. R., Kraeplel, A. M. L., and Morel, F. M. M.: Unicellular C_4 photosynthesis in a marine diatom, Nature, 407, 996–999, doi: 10.1038/35039612, 2000.

Reinfelder, J. R., Milligan, A. J., and Morel, F. M. M.: The role of the C_4 pathway in carbon accumulation and fixation in a marine diatom, Plant Physiol., 135, 2106–2111, doi:10.1104/pp.104.041319, 2004.

Scotese, C. R., Song, H., Mills, B. J. W ., Douwe G., and van der Meer, D. G.: Phanerozoic paleotemperatures: The earth's changing climate during the last 540 million years, Earth-Sci. Rev., 215, 103503, doi: 10.1016/j.earscirev.2021.103503, 2021.

Sepkoski Jr., J. J.: Mass extinctions in the Phanerozoic oceans: A review, Geological Implications of Impacts of Large Asteroids and Comets on the Earth, in edited by: Silver, L. T. and Schultz, Geol. Soc. Am. Spec. Pap., 190, 283–289, 1982.

Sepkoski Jr., J. J.: Patterns of Phanerozoic extinctions: A perspective from global data bases, in: Global Event Stratigraphy, edited by: Walliser, O. H., Springer-Verlag, Berlin, Heidelberg, Germany, 35–52, 1996.

Sherwood, S. C. et al.: An assessment of Earth's climate sensitivity using multiple lines of evidence, Reviews of Geophysics. https://doi.org/10.1029/2019RG000678, 2020.

Singh, R. K. and Sharma, R. V.: Numerical analysis for ground temperature variation, Geotherm Energy 5, 22, doi: 10.1186/s40517-017-0082-z, 2017.

Somero, G. N.: Proteins and temperature, Ann. Rev. Physiol., 57, 43-68**,** doi: 10.1146/annurev.ph.57.030195.000355, 1995.

Sperling, E. A., Halverson, G. P., Knoll, A. H., Macdonald, F. A. & Johnston, D. T. A basin redox transect at the dawn of animal life. Earth Planet. Sci. Lett. 371–372, 143–155 (2013).

Sperling, E. A., Wolock, C. J., Morgan, A. S., Gill, B. C., Kunzmann, M., Halverson, G. P., Macdonald, F. A., Knoll, A. H., and Johnston, D. T.: Statistical analysis of iron geochemical data suggests limited late Proterozoic oxygenation, Nature, 523, 451–454, doi:10.1038/nature14589, 2015.

Sun, Y., Joachimski, M. M., Wignall, P. B., Yan, C., Chen, Y., Jiang, H., and Lai, X.: Lethally hot temperatures during the Early Triassic greenhouse, Science, 338, 366–370, doi: 10.1126/science.1224126, 2012.

Sunday, J. M., Bates, A. E., and Dulvy, N. K.: Global analysis of thermal tolerance and latitude in ectotherms, Proc. R. Soc., B 278, 1823–1830, doi: 10.1098/rspb.2010.1295, 2011.

Torsvik, T. H., Royer, D. L., Marcilly, C. M., and Werner, S. C.: User-friendly carbon-cycle modelling and aspects of Phanerozoic climate change, Applied Computing Geosci., 23, 100180, doi:10.1016/j.acags.2024.100180, 2024.

Toussaint, A., Brosse, S., Guillermo Bueno, C., Pärtel, M., Tamme, R.,and Carlos P. and Carmona, C. P.: Extinction of threatened vertebrates will lead to idiosyncratic changes in functional diversity across the world, Nat. Commun., 12, 5162, doi:org/10.1038/s41467-021-25293-0, 2021.

Upchurch, G. R. Jr, Otto-Bliesner, B. L., and Scotese, C.: Vegetation−atmosphere interactions and their role in global warming during the latest Cretaceous, Phil. Trans. R. Soc. Lond., B 353, 97–112, 1998.

Vellekoop, J., Sluijs, A., Jan Smit, J., Stefan Schouten, S., Weijers, J. W. H., Jaap S Sinninghe Damsté, J. S., and Henk Brinkhuis, H.,: Rapid short-term cooling following the Chicxulub impact at the Cretaceous-Paleogene boundary, Proc. Nat. Acad. Sci. USA, 111, 7537–7541, doi:10.1073/pnas.1319253111, 2014.

Vérard, C.: On greenhouse and icehouse climate regimes over the Phanerozoic, Terra Nova, 36, 292–297, doi: 10.1111/ter.12711, 2024.

Wolf, E. T., Shields, A. L., Kopparapu, R. K., Haqq-Misra, J., and Toon, O. B.: Constraints on climate and habitability for earth-like exoplanets determined from a general circulation model, Astrophys. J., 837, 107–117, doi:10.3847/1538-4357/aa5ffc, 2017.

Wolf, E. T. and Toon, O. B.: The evolution of habitable climates under the brightening Sun, J. Geophys. Res., 120, 5775–5794, doi: 10.1002/2015JD023302, 2015.

Yoshida, M.: Formation of a future supercontinent through plate motion–driven flow coupled with mantle downwelling flow. Geology, 44, 755–758, doi:10.1130/G38025.1, 2016.